

# High-Resolution Spectroscopy in Tr37: Gas Accretion Evolution in Evolved Dusty Disks<sup>1</sup>

Aurora Sicilia-Aguilar<sup>2</sup>, Lee W. Hartmann<sup>3</sup>,

Gábor Fűrész<sup>4,5</sup>, Thomas Henning<sup>2</sup>

Cornelis Dullemond<sup>2</sup>, Wolfgang Brandner<sup>2</sup>

sicilia@mpia.de

## ABSTRACT

Using the Hectochelle multifiber spectrograph, we have obtained high-resolution ( $R \sim 34,000$ ) spectra in the  $H\alpha$  region for a large number of stars in the 4 Myr-old cluster Tr 37, containing 146 previously known members and 26 newly identified ones. We present the  $H\alpha$  line profiles of all members, compare them to our IR observations of dusty disks (2MASS/JHK + IRAC + MIPS  $24\mu\text{m}$ ), use the radial velocities as a membership criterion, and calculate the rotational velocities. We find a good correlation between the accretion-broadened profiles and the presence of protoplanetary disks, noting that a small fraction of the accreting stars presents broad profiles with  $H\alpha$  equivalent widths smaller than the canonical limit separating CTTS and WTTS. The number of strong accretors appears to be lower than in younger regions, and a large number of CTTS have very small accretion rates ( $\dot{M} \leq 10^{-9} M_{\odot}/\text{yr}$ ). Taking into account that the spectral energy distributions are consistent with dust evolution (grain growth/settling) in the innermost disk, this suggests a parallel evolution of the dusty and gaseous components. We also observe that about half of the “transition objects” (stars with no IR excesses at  $\lambda \leq 6 \mu\text{m}$ ) do not show any signs of active accretion, whereas the other half is accreting with accretion rates  $\leq 10^{-9} M_{\odot}/\text{yr}$ . These zero or very low accretion rates reveal important gas evolution and/or gas depletion in the innermost disk, which could be related to grain growth up to planetesimal

---

<sup>2</sup>Max-Planck-Institut für Astronomie, Königstuhl 17, 69117 Heidelberg, Germany

<sup>3</sup>University of Michigan, 830 Dennison 500 Church St., Ann Arbor, MI 48109

<sup>4</sup>Center for Astrophysics, 60 Garden Street, Cambridge, MA 02138

<sup>5</sup>University of Szeged, Department of Experimental Physics, Dom ter9, H-6723 Szeged, Hungary

or even planet sizes. Finally, we examine the rotational velocities of accreting and non accreting stars, finding no significant differences that could indicate disk locking at these ages.

*Subject headings:* accretion disks — line: profiles — stars: pre-main sequence — stars: rotation — planetary systems: protoplanetary disks

## 1. Introduction

Multiple observations in the past few decades have confirmed that low-mass stars are born surrounded by relatively dense and optically thick circumstellar disks, due to the conservation of angular momentum during the contraction of the cores in a molecular cloud (Lynden-Bell & Pringle 1974; Appenzeller & Mundt 1989; among others). These optically thick, accretion disks are one of the main characteristics of very young, pre-main sequence stars. More than 80% of the low-mass stars aged  $\sim 1$  Myr have accreting disks, with accretion rates around  $10^{-8} M_{\odot}/\text{yr}$  (Hillenbrand et al. 1995; Haisch et al. 2001; Gullbring et al. 1998). By the age of  $\sim 4$  Myr, disk fractions drop to around  $\sim 45\%$ , and accreting disks are a rare feature in regions aged  $\sim 10$ -12 Myr (Strom et al. 1989; Skrutskie et al. 1990; Lada et al. 2000; Carpenter et al. 1990; Armitage et al. 2003; Sicilia-Aguilar et al. 2006), suggesting that most of the disk dissipation (and probably planet formation) occurs within 1-10 Myr (Haisch et al. 2001; Bergin et al. 2004; Forrest et al. 2004; D’Alessio et al. 2005; Sicilia-Aguilar et al. 2006). Moreover, the changes in the spectral energy distributions (SEDs) at these ages suggest that important dust evolution (via grain growth and/or dust settling) is taking place during these ages (Sicilia-Aguilar et al. 2006).

According to the presence of disks and accretion, young pre-main sequence stars are typically classified as classical T-Tauri stars (CTTS) or weak-lined T-Tauri stars (WTTS). This differentiation is based on the presence or absence of accretion, normally inferred from strong emission lines in CTTS (mostly  $H\alpha$ ,  $H\beta$ , see Herbig et al. 1996; Muzerolle et al. 1998a, 2001), in contrast to the weak chromospheric lines in WTTS (Appenzeller & Mundt 1989; White & Basri 2003). UV observations reveal that CTTS tend to have UV excesses that can be explained by an accretion shock (Calvet & Gullbring 1998; Gullbring et al. 1998) and near-IR excesses that suggest the presence of dusty optically thick disks (Haisch et al. 2001 among others). Therefore, CTTS (or Class II objects) are supposed to have

---

<sup>1</sup>Observations reported here were obtained at the MMT Observatory, a joint facility of the Smithsonian Institution and the University of Arizona.

optically thick accretion disks, whereas WTTS (or Class III objects) are assumed to be diskless or “naked” (Bertout 1989; Hartigan et al. 1990) or to have optically thin “debris” disks (Lada 1987; André & Montmerle 1994). Nevertheless, some observations suggest that some weak-line stars may not be “true” WTTS since they are sometimes found to have optically thick disks (Gregorio-Hetem & Hetem 2002; Littlefair et al. 2004). Recent studies taking advantage of new-generation instruments (like the Spitzer Space Telescope) have revealed more of these objects in which inner dusty disks are dissipated and/or suffer strong dust coagulation/sedimentation (reducing drastically the emission in near- and mid-IR), and accretion phenomena are not present or are reduced to very low rates. These objects would belong to an intermediate and rapid transitional phase during which gaps open in the disk, and accretion drops by several orders of magnitude or ceases completely (see the cases of TW Hya, Calvet et al. 2000, Uchida et al. 2004; and CoKu Tau/4, Forrest et al. 2004, D’Alessio et al. 2005, among others). Since these “transition objects” are very rare, the suggested timescales for complete dissipation/agglomeration into large grains of the rest of the outer disk are very fast (from  $\sim 10^5$  yr to less than 1 Myr), but the timescales for gap opening, and the way accretion terminates remain uncertain because of the lack of large samples of “transition objects” at different ages and evolutionary stages. Older regions with many transitional disks are therefore very interesting places to search for hints of planet formation, as this rapid phase could be intimately related to the formation of planets (Lin and Papaloizou 1986; Bryden et al. 2000; Quillen et al. 2004).

One of the best places to find a larger sample of evolved disks and “transition objects” is the cluster Tr 37 in the Cep OB2 association (Platais et al. 1998). Located at 900 pc distance (Contreras et al. 2002) and aged  $\sim 4$  Myr (Sicilia-Aguilar et al. 2005), Tr 37 has been studied extensively at multiple wavelengths using some of the new-generation instruments like the Spitzer Space Telescope and the multifiber spectrograph Hectospec (Sicilia-Aguilar et al. 2004, 2005, 2006; from now on Paper I, Paper II, and Paper III, respectively). Low-resolution spectra revealed an important low-mass population ( $\sim 160$  stars with spectral types mid-G to M2), of which approximately 45% show excesses characteristic of disks (Paper III). In most cases, the presence of a disk is well-correlated with the presence of accretion derived from U band photometric excesses and/or the strong  $H\alpha$  equivalent width (EW) from low-resolution spectra (Paper II, Paper III). Nevertheless, the disks in Tr 37 appear more evolved than the disks observed in younger regions (i.e. Taurus), since more than 90% of them show a significant decrease of emission at shorter IR wavelengths, consistent with grain growth and/or dust settling in the innermost disk (Paper III). This lower near-IR excess is accompanied in many cases by a small accretion rate (presumably  $\leq 10^{-9} M_{\odot}/\text{yr}$ ) and/or a small  $H\alpha$  EW. In about 10% of the total number of disks, there is no near-IR excess: These are the “transition objects”, which do not present IR excesses at wavelength

shorter than  $5.8 \mu\text{m}$  and have moreover no evidence of accretion or very low accretion rates. These objects are likely to have  $\sim 1$  AU gaps in their inner dusty disks, but have otherwise CTTS-looking optically thick disks at larger distances (as inferred from mid-IR excesses at longer wavelengths; Paper III). Therefore, Tr 37 is a unique region to study accretion in very evolved and “transitional objects”, the end of the accretion activity, and the processes leading to gap opening.

In this context, we targeted a large number of stars in Tr 37 with the high-resolution multifiber spectrograph Hectospec at the MMT. Since very low accretion rates ( $\sim 10^{-9} - 10^{-10} M_{\odot}/\text{yr}$ ) are not always detectable via U band excesses (Paper II) and produce small  $H\alpha$  EW, high-resolution  $H\alpha$  spectroscopy is probably the best method to determine the presence of accretion in evolved disks. High-resolution  $H\alpha$  spectra reveal not only the EW of the line, but its broadening due to magnetospheric accretion (Hartmann 1998; Muzerolle et al. 1998a,b, 2001), providing a direct proof of accretion or non-accretion even at rates between  $10^{-10}$  and  $10^{-12} M_{\odot}/\text{yr}$ . In addition, high-resolution spectra can be used to obtain radial and rotational ( $V\sin i$ ) velocities, which help to refine the membership and to study the evolution of angular momentum in older stars, and whether the rotation rate is correlated to accretion, as suggested by the disk locking theories (Shu et al. 1994; Choi & Herbst 1996; Hartmann 2002, among others). In Section 2 we describe the data taking and processing, Section 3 presents the results concerning accretion and rotation, Section 4 contrasts these result with our previous optical and IR observations, and we finally list our concluding remarks.

## 2. Observations and data reduction

Hectochelle is the high-resolution, multifiber echelle spectrograph, which operates at the wide-field mode of the Cassegrain 6.5m MMT telescope in Mount Hopkins, AZ (Szentgyorgyi et al. 1998; Fabricant et al. 2004). The fiber array is shared between the low-resolution spectrograph Hectospec, and the high-resolution Hectochelle. Hectochelle can obtain up to 240 simultaneous spectra within a 1 degree field of view, using all the available 240 fibers. The fibers are  $250 \mu\text{m}$  in diameter, subtending 1.5 arcsec on the sky. We used the spectral order centered in  $H\alpha$ , which has an approximate width of  $180 \text{ \AA}$  and a resolution of  $R \sim 34,000$ . This is the same configuration we used in our  $H\alpha$  study of the Orion Nebula Cluster, ONC, (Sicilia-Aguilar et al. 2005).

We observed two fields in Tr 37 during two engineering runs on December 1st, 2004 and December 2nd, 2004. A total of 231 and 233 objects were observed in the configurations, respectively. The objects were selected giving special priority to previously known members

with apparent contradictions between the signs of accretion ( $H\alpha$  EW, U band excess; Paper I,II) and IR excesses consistent with disks (Paper III), followed by probable members with noisy low-resolution spectra, and the rest of the bona-fide members (see Paper II). A total of 146 previously known members and lower-probability members were observed. The remaining fibers were allocated in order to observe the maximum number of potential cluster members, which had been identified via optical and infrared photometry, but were never observed in our spectroscopy campaigns to determine membership (see the procedures described in Paper II to obtain the best candidates for spectroscopy). The total exposure time was 90 min (divided in 3 x 30 min exposures) for the field observed in the first night, and 60 min (divided in 3 x 20 min exposures) for the field observed during the second night. Due to time limitations during the engineering run, the offset sky exposures planned (Paper II) were too short and noisy to be usable. Nevertheless, the subtraction of the background nebular  $H\alpha$  is possible when the stellar component is broad, as the narrow  $H\alpha$  nebular emission can be identified, fitted and subtracted (Muzerolle et al. 1998b; Sicilia-Aguilar et al. 2005). For the narrow-lined stars, no background subtraction was possible, therefore, we do not use the  $H\alpha$  as a requirement for membership, establishing it via Li absorption in our low-resolution spectra (Paper I, II), or using radial velocities (in the case of the new members).

The data were reduced according to standard procedures, using IRAF<sup>2</sup> and the tasks available under the packages *mscred* and *specred*. The spectra were flattened and extracted using a dome flat and the tasks *apdefault* and *apflatten*, defining fibers and background interactively. Apertures were organized separating odd and even numbers (due to a shift in wavelength), and each group was calibrated in wavelength using ThAr comparison spectra. As mentioned previously, no background subtraction could be done due to the lack of appropriate offset background spectra during this engineering run. The difficulties of subtracting the nebular emission in highly variable H II regions prevents us from using the sky spectra obtained with the fibers not assigned to objects (Paper I, Paper II). Therefore, the background subtraction for the  $H\alpha$  line was done manually in the cases where it was possible to distinguish the background, nebular, narrow component, from the broad  $H\alpha$  component (which are most of the broad-lined stars). The individual spectra were displayed using IRAF task *splot*, and the narrow component was visually identified, fitted to a gaussian, and subtracted. For most of the stars with broad profiles, this procedure does not introduce significant errors in the measurement of the EW, measured with the IRAF task *splot*. In the case where the nebular  $H\alpha$  was successfully subtracted, we used *splot* to measure the  $H\alpha$  velocity width at

---

<sup>2</sup>IRAF is distributed by the National Optical Astronomy Observatories, which are operated by the Association of Universities for Research in Astronomy, Inc., under cooperative agreement with the National Science Foundation

10% of the maximum. The  $H\alpha$  EW and 10% width, as well as the labels of broad and narrow  $H\alpha$  profiles, are given in Table 1. Examining the 16 background spectra obtained with the non-assigned fibers, we find that the  $H\alpha$  nebular emission is always narrow and variable in intensity, even though in a few cases a blueshifted or redshifted narrow absorption is present, in addition to the emission. It is worth to note that these absorptions could be responsible for the absorption observed in a few of the cluster members, being especially visible in the case of narrow-lined stars.

Finally, radial and rotational velocities for the observed stars were obtained via cross-correlation with similar spectral type standards observed with Hectochelle. As for our ONC study (Sicilia-Aguilar et al. 2005), we used the IRAF task *xcsao*, available within the *rvsao* package (see Kurtz et al. 1992; and the *xcsao* documentation in [tdc-www.cfa.harvard.edu/iraf/rvsao/xcsao](http://tdc-www.cfa.harvard.edu/iraf/rvsao/xcsao)). This routine obtains the radial velocity from the shift of the cross-correlation peak, and its broadening is used to calculate the rotational velocity. In all cases, the  $H\alpha$  region and the NII lines were removed from the spectra before the cross correlation, as we did in our previous work on the ONC (Sicilia-Aguilar et al. 2005). The errors depend on the signal-to-noise of the cross correlation and on the width of the peak, and the parameter R is an indication of the goodness of the cross-correlation and its errors (Tonry & Davis 1979; Hartmann et al. 1986). The error in the rotational velocity is proportional to a constant multiplied by  $1/(1+R)$  (Kurtz et al. 1992), and in general it can be estimated as the rotational velocity itself divided by  $(1+R)$  (Hartmann et al. 1986), so values of R near 1 indicate very uncertain rotational velocities (for a more detailed explanation of the errors for Hectochelle spectra, see Fűrész et al. 2006). Due to small tilts in the fibers during the construction of the spectrograph, an extra source of error affects the wavelength calibration and, therefore, the radial velocity measurements. The fiber tilts produce a variation in the radial velocity that can be up to 0.6-0.8 km/s considering all the fibers, and a variation up to 3 km/s in the  $V\sin i$ , both depending on the region of the spectrum (Fűrész et al. 2006). Even though in most cases here the signal-to-noise ratio (S/N) dominates the error, these extra variations in the tilt may be taken into account to explain the dispersion of the radial velocities in the cluster. Because of the time limitations imposed during this engineering run, we could obtain good cross-correlations and velocity estimates for about 75% of the observed stars (133 members and potential members) with good S/N. The radial and rotational velocities as well as the R signal-to-noise parameter of the cluster members and potential members are listed in Table 1.

### 3. Results

Figures 1 to 8 show the  $H\alpha$  profiles of the previously known and newly identified members and probable members, together with their SEDs from Paper III, that will be discussed in detail in Section 3.3. A total of 146 of the  $\sim 166$  Tr 37 previously known members and probable members were observed with Hectochelle, including 9 objects with uncertain membership. Membership is revised in Section 3.2, where we also analyze the potential members selected among optical and infrared candidates. Table 1 lists the previous and new spectroscopic information, the  $H\alpha$  EW and the full width measured at 10% intensity (when the nebular emission was successfully subtracted), and the membership (based on this and on our previous studies).

#### 3.1. $H\alpha$ emission: line profiles, EW, and accretion

The presence of active magnetospheric accretion can be inferred observing the emission lines in young stars, especially the  $H\alpha$  emission. The large velocities of the material involved in the magnetospheric accretion processes produce strong emission lines with broad velocity wings, usually larger than  $\pm 100 \text{ km s}^{-1}$  (Reipurth et al. 1996; Hartmann 1998; Muzerolle et al. 1998a, 2001; White & Basri 2003; Bonnell et al. 1998). In general, accretion rates over  $10^{-12} \text{ M}_{\odot}/\text{yr}$  result in broad  $H\alpha$  velocity wings (Muzerolle et al. 2003), compared to the  $10^{-9}$ - $10^{-10} \text{ M}_{\odot}/\text{yr}$  limit imposed by the detection of U band excesses (see Paper I,II and Section 4.2).  $H\alpha$  emission is produced as well in the chromosphere of young, non-accreting stars, but in this case, the line is narrow and does not present high velocity wings (Appenzeller & Mundt 1989). Therefore, the distinction between accreting and non-accreting stars (defining “non-accreting” as showing  $H\alpha$  emission similar to the diskless WTTS or Class III objects; see Section 4.2 for details) becomes clear from high-resolution spectra.

Examining the  $H\alpha$  profiles, we can observe the different characteristics related to accretion (Reipurth et al. 1996; Muzerolle et al. 1998a, 2001): high-velocity wings revealing accretion velocities that can be sometimes larger than  $300 \text{ km/s}$  (see the profiles of 11-2037, 13-277, 93-720 and 93-261 among others), blue-shifted and red-shifted absorption features (11-2322, 12-1091, 13-277, 13-1048, 21402192+5730054, among others), and inverse P-Cygni profiles characteristic of low accretion rates (11-2031, 13-1250). The most common profile is characterized by a blue-shifted absorption, although red-shifted absorption and absorption with no velocity shift are also observed, as well as several symmetric profiles, and 3 cases of inverse P-Cygni profiles (always related to objects with very low accretion rates). The characteristics of broad  $H\alpha$  profiles are listed in Table 2. Comparing with the spectra obtained for the younger ( $\sim 1 \text{ Myr}$ ) ONC stars (Sicilia-Aguilar et al. 2005), the profiles are

similar, but it is worth to note the lower number of very strong emission line stars with large velocity wings in the 4 Myr-old Tr 37, as well as the smaller  $H\alpha$  EW of the broad-lined stars. Given that the spectral types of the stars range from mid-G to M2 in both samples, being roughly comparable, the observed differences should be related mainly to accretion and disk evolution.

It is interesting to note the cases of stars like 73-311, 21362507+5727502, 11-2131, 14-1017 and 13-819, among others, for which the broadening of the  $H\alpha$  profiles is relatively small, showing velocities around only  $\pm 100$  km/s, but visibly larger than for non accreting stars (Muzerolle et al. 2003; Natta et al. 2004). Their EW are in the lower limit for distinguishing CTTS from WTTS or even below, so they would be classified as WTTS attending to the EW (White & Basri 2003). Low  $H\alpha$  EW can be also found among some of the stars showing inverse P-Cygni profiles, characteristic of low accretion rates (Muzerolle et al. 1998a,b). This is the case of 21402192+57300054 (EW =  $-4 \text{ \AA}$ <sup>3</sup>, spectral type K6) and 13-1250 (EW =  $-4 \text{ \AA}$ , spectral type K4.5). The small EW in these broad- $H\alpha$  (and thus, accreting) stars accounts for the apparent contradictions between the presence of U and IR excesses and the measurement of a “weak”  $H\alpha$  EW from low-resolution spectroscopy (Paper I, II; we will discuss the relation between IR excesses and accretion in Section 3.3 in more detail). To summarize, the EW values for accreting stars range from  $-2$  to  $-80 \text{ \AA}$  approximately, with an average EW is  $-27 \text{ \AA}$  with a median value of  $-20 \text{ \AA}$  and a standard deviation of  $19 \text{ \AA}$  (due to the large differences in EW present in the sample).

With the high-resolution spectra, we are also able to detect the presence of an accreting spectroscopic binary with double lines (SB2), 82-272, with EW =  $-7$  and  $-8 \text{ \AA}$  for each of the components, respectively. The double-peaked profile of 24-1796 could be indicative of another accreting binary, even though given the smaller offset of the two peaks, the binarity is not so evident in this case. Finally, the wavelength offset for the broad  $H\alpha$  in 12-1968 may suggest a binary containing an accreting and a non-accreting component. No other SB2 are evident within this sample. We also want to mention the broad blueshifted absorption seen in the two spectra taken for 12-94, a K4 weak-lined star whose membership is uncertain (from both Li detection and radial velocity). Finally, there are some (mostly low S/N) objects, for which the width of the  $H\alpha$  line is not clear. These objects are marked with the uncertainty flag in Table 1, and due to the absence of near-IR excess and other signs of accretion in most of them (see Section 3.3), we presume they are likely to be narrow-lined, non-accreting WTTS. Followup of these objects would be highly recommendable, especially in the case of 73-758, which has a SED typical of a “transition object” (see Section 4.1 for a more detailed

---

<sup>3</sup>Negative values of the EW stand for emission.



description).

### 3.2. Membership and dynamics

As we mentioned previously, the membership (or probable membership) of 146 objects was determined previously using low-resolution spectra (Paper I, Paper II) to detect the presence of Li 6707Å absorption, the presence of H $\alpha$  emission (both characteristic of young stars), and the spectral type and extinction (found to be consistent with the cluster). The broad H $\alpha$  profiles in the Hectochelle data is another proof of membership that allows us to confirm the accreting known members, and to identify 7 new ones. Due to the presence of unsubtracted nebular H $\alpha$ , we cannot establish the membership of the stars with narrow H $\alpha$  emission via their H $\alpha$  emission only (this would be otherwise a criterion for detecting new WTTS members, since H $\alpha$  chromospheric emission is another sign of youth, see Hartmann 1998 among others). Nevertheless, comparing the radial velocities of the newly observed members to the radial velocities of the previously known members and stars with broad H $\alpha$  lines, we can determine the membership of the rest of newly observed objects, and check the cases of dubious membership.

Figure 9 shows the radial velocity histogram of the cluster members. Taking into account only the “sure” members (with membership confirmed via clear Li 6707 Å absorption and/or by the presence of broad H $\alpha$  emission in the high-resolution spectra), and considering only the high S/N cross-correlations ( $R > 4$ ; 37 stars in total), we can estimate the average cluster radial velocity to be  $cz = -15.0 \pm 3.6$  km/s, where the velocity dispersion is  $\Delta V = 3.6$  km/s. Note that for this calculation we excluded the stars with large offsets in Figure 9, as they are likely to be single-line spectroscopic binaries (SB1). This velocity dispersion accounts in part for the real expansion velocity of the cluster, but it is largely affected by the individual errors (which are typically 1-2 km/s) and by the  $\sim 0.6$ - $0.8$  km/s extra error mentioned in Section 2). Taking into account the known members and the total number of observed stars, we can estimate the probability of being a member if the radial velocity of the object falls within a certain number of sigmas from the cluster average radial velocity. If we assume equal probabilities for a random star to have a certain radial velocity, counting the number of stars observed and the number of known members, we could estimate the “average number of stars” that would fall randomly within the 1, 2 and 3 sigma bins, and compare it to the number of known members. This way, we can estimate the stars within the  $1 \times \Delta V$  bin to have a probability of around  $\sim 90\%$  of being cluster members, a probability of being member of  $\sim 75\%$  if the star falls within  $1-2 \times \Delta V$ , and a probability of  $\sim 40\%$  of being member if the star falls within the  $2-3 \times \Delta V$  bin. These are only approximate values, and membership

may be more uncertain for the stars with low  $R$ , so we define the stars within  $1 \times \Delta V$  to be “sure members” (named ‘Y’ in Table 1), the stars within  $2-3 \times \Delta V$  to be “probably members” (‘P’), and the stars within  $2-3 \times \Delta V$  to be “probably non-members” (‘PN’). We give in any case priority to the membership established from Li absorption, from the presence of clear IR/Spitzer excess, or from the broad  $H\alpha$  emission from the high-resolution spectra. The stars with certain membership, good correlations and high non-cluster radial velocities are likely to be single-line binaries (SB1) or probable SB1 (when the cross correlation has large errors and/or the radial velocity is off but very close to the cluster velocity), see Table 1.

With this procedure, we have identified a total of 14 new sure members (labeled ‘Y’), 9 probable members (‘P’), and 9 probable non-members or lower-probability candidates (‘PN’). Among these new members, 5 could be confirmed based on their strong  $H\alpha$  emission (2 of them being sure members, 2 probable members, and 1 low-probability member). Using radial velocities, we have revised the stars with dubious membership. These stars had low S/N low-resolution spectra, which did not allow us to determine clearly the presence of Li 6707Å absorption, or are G stars, for which the smaller Li EW was under our detection limit (Paper I, II). Radial velocities confirm the membership of 13-350, 13-1891 and 24-820. On the other hand, 11-581 and 12-94 show non-cluster radial velocities, being probably non-members or SB1 (we reject them as members in order to be conservative). For the rest of dubious members (14-306, 11-1067, 12-583 and 12-1613), the S/N in the high-resolution spectra does not let us obtain accurate radial velocities, so we cannot confirm nor reject them. Summarizing, and naming as safe all objects with strong  $H\alpha$ , Li detection (in low-resolution spectra) and/or radial velocities within the  $1\sigma$  region (‘Y’), we have 157 sure members, 11 probable members, 8 low-probability members, and 2 non-members (rejected from the initial sample in Paper II).

Taking into account the errors in the radial velocity dispersion, we are approximately at the edge of being able to detect the true velocity dispersion or expansion of the cluster. Our main limitation is the poor S/N resulting in large errors in the individual radial velocities, which are up to 1-2 km/s even in the cases with  $R > 4$ . Considering the estimated mass of the cluster from the estimated number of cluster members ( $\sim 300$  members, or  $M \sim 300 M_\odot$  in the bulk of the cluster, see Paper III), and its size ( $\sim 4$  pc radius for the bulk of the population, Paper II), it is most likely unbounded and expanding (Spitzer 1984). The radius of the bulk (4 pc) is consistent with the expected size after 4 Myr, assuming a typical velocity dispersion of  $\sim 1$  km/s. Nevertheless, the Tr 37 region is likely to have triggered at least one population, aged about 1 Myr, in the globule (at distances 4-5 pc from the cluster center; Paper II, III), and maybe another associated population about 5-6 pc North (Paper II, III), while expanding in a non-uniform way. Given the precision of our radial velocities, and the reduced number of stars in these two populations, we are unable to detect any difference in

their radial velocities at this point.

### 3.3. Accretion versus IR excess

According to Figures 1 to 8, the agreement between the presence of broad  $H\alpha$  emission and the detection of an IR excess is remarkable. It can be also noted that the brighter disks (stronger IR excesses with respect to photospheric levels at all wavelengths, resembling younger disks) and the SEDs with strong U excesses are normally associated to the strongest and broadest  $H\alpha$  emission lines (see 13-277, 12-236, 13-1877 among others), as we would expect if the evolution of the accretion processes proceeds in parallel to the evolution of the dusty disk. In general, the high-resolution  $H\alpha$  spectra solve the apparent contradiction between small  $H\alpha$  EW (according to White & Basri 2003, WTTS have  $EW < 10\text{\AA}$  in emission for spectral types K6-M2, and  $EW < 3\text{\AA}$  in emission for spectral types K5-G) and the presence of an IR excess that we found in Paper II and Paper III. Indeed, the puzzling stars from Paper III have all very small  $H\alpha$  EW, so they would be classified as WTTS according to White & Basri (Paper III), if the high velocity wings were not resolved. These are the objects 11-1209 (spectral type K6,  $EW = -6/-4\text{\AA}$  from high- and low-resolution spectra, respectively), 12-1968 (K6,  $EW = -8/-11\text{\AA}$ ), 13-819 (K5.5,  $EW = -6/-10\text{\AA}$ ), 13-1048 (M0,  $EW = -8/-7\text{\AA}$ ), 13-1250 (K4.5,  $EW = -4/-2\text{\AA}$ ), 21402192+5730054 (K6,  $EW = -4/-8\text{\AA}$ ), and 93-540 (M0,  $EW = -5/-18\text{\AA}$ ). The small EW suggest low accretion rates, as we will present in Section 4.2.

There is a good agreement between the measured  $H\alpha$  EW from high- and low-resolution spectra (Figure 10). The observed variations of the  $H\alpha$  EW are consistent with the typical variability observed in the ONC (Sicilia-Aguilar et al. 2005; note that some very large  $EW \sim -60$  to  $-100\text{\AA}$  found in low-resolution spectra are due to low signal-to-noise resulting in a poor continuum estimate). The CTTS with small EW represent a small fraction of the total sample, suggesting that the classification of White & Basri (2003) successfully distinguishes accreting (CTTS) and non-accreting (WTTS) stars in more than 90% of the cases. Therefore, an  $H\alpha$  EW survey is probably good enough to determine accretion in very young regions, which contain a large number of accreting stars with relatively large accretion rates and large EW. In older regions (like Tr 37), where the accretion fraction and the accretion rates are much smaller, determining accretion by  $H\alpha$  EW alone is uncertain, so it should be combined with high-resolution spectroscopy and/or near- and mid-IR observations.

Despite the general good agreement of IR excesses with high-velocity wings in the  $H\alpha$  line, there are a few cases for which the conflict could not be resolved. Some of these cases are the “transition objects” (see Paper III), which we discuss extensively in Section 4.1, since

about half of them, despite having (outer, optically thick) disks, are most likely not accreting. Two other “contradictory” objects have apparently normal IR excesses and no strong  $H\alpha$  velocity wings. Due to the discrepancies between the high- and the low-resolution spectra taken in former campaigns, and due to the fact that the spectra are very noisy and weak, we believe that an small position offset in the Hectochelle fibers may have occurred in some of the cases. These offsets, although unlikely, may occur in a couple of fibers in each Hectochelle setup, so the low number of conflicting spectra is consistent with the offset hypothesis. These stars with contradictory low- and high-resolution spectra are 21364596+5729339 (classified as a class I object, no spectral type given due to heavy veiling,  $H\beta$  in emission was clearly detected, as well as some broadening of  $H\alpha$  even at 5 Å resolution) and 14-335 (EW = -18 Å in the low-resolution spectra,  $H\beta$  in emission and Li 6707 Å in absorption were clearly detected with Hectospec). An offset occurred during the Hectochelle run would explain the extremely low S/N of 14-335 (we would be observing mostly the background), and the relatively luminous Hectochelle spectrum in 21364596+5729339 would mostly contain the emission lines from the globule in the surroundings of the star.

The stars 14-160 (spectral type K5) and 23-162 (K7) show strong  $H\alpha$  with very small velocity wings, which resemble the spectra of WTTS, although the intensity of the  $H\alpha$  emission is much higher than the emission of the normal WTTS and the nebula. They show very strong but relatively narrow  $H\alpha$  emission, with no velocity wings extended beyond  $\pm 50$ -80 km/s. Their low-resolution spectra present  $H\beta$  and  $H\gamma$ , and  $H\alpha$  EW = -22 Å and -7 Å for 14-160 and 23-162, respectively. There is no evidence of contamination nor large errors in their IRAC/MIPS photometry, and the nearby spectra show weak nebular emission that cannot account for the strong and narrow  $H\alpha$  observed in these two stars. The small EW and the lack of U band excesses suggest very small accretion rates. A configuration where the  $H\alpha$  profile appears narrow despite accretion is rare, requiring a special geometry and/or view angle, and a small accretion rate (at least  $10^{-10}$   $M_{\odot}$ /yr or less, see Muzerolle et al. 1998a, 2003). Nevertheless, our sample is large enough to be likely to contain some of these rare profiles. Note that accretion rates under  $10^{-12}$   $M_{\odot}$ /yr would not produce line broadening, although given the “normal” disk emission of these two stars, such low rates would be rare (Muzerolle et al. 2003).

Less than 5% of the objects (the stars 91-155, 12-2519, 22-1418, 53-176 and 54-1781) show an apparent contradiction between the presence of narrow  $H\alpha$  and a normal-looking disk. Their low-resolution spectra show  $H\beta$  emission for 91-155 and 12-2519, even though the  $H\alpha$  EW typical of WTTS, which would indicate no accretion. Contamination by a nearby star is likely for the star 91-155, which shows an offset in its IR data with respect to the optical information (our IRS spectra seem to confirm the presence of a disk that may belong to the companion, Sicilia-Aguilar et al. in preparation). For all the other cases, the presence

of nearby stars and/or small patches of nebulosity makes uncertain the IRAC photometry. The stars 12-1009 and 13-232 show intrinsic large errors in their IRAC photometry, so the presence of a disk is highly uncertain (Paper III).

We only find 1 object with no IR excess and some broad  $H\alpha$  emission, 13-819. This K5.5 star does not have any excess up to  $8\mu\text{m}$ , but since it is relatively faint, an excess at  $24\mu\text{m}$  of less than  $\sim 20$  times the photospheric level would be undetectable with our MIPS photometry. The lack of  $8\mu\text{m}$  excess suggests that the silicate feature is very faint or absent (as the  $8\mu\text{m}$  IRAC band covers nearly up to  $10\mu\text{m}$ ), suggesting a strong depletion of small grains at distances close to the star, and a gap  $> 5$  AU. Its small  $H\alpha$  EW is consistent with the very small accretion rate detected with U band ( $\dot{M}=4\times 10^{-10}$ - $2\times 10^{-9}$   $M_{\odot}/\text{yr}$ ). Given that the  $24\mu\text{m}$  band traces material at distances around 10-20 AU (depending on spectral type), this would suggest that accreting stars with inner gaps of 10-20 AU are extremely rare (around 1% of the total number of disks,  $\sim 0.5\%$  of the total number of members), have very short lifetimes (about ten times shorter than the typical lifetimes for “transition objects” with few-AU gaps), and/or have extremely weak accretion rates (undetectable in  $H\alpha$ ,  $\dot{M}<10^{-12}$   $M_{\odot}/\text{yr}$ ). Observations at longer wavelengths would be an interesting continuation of this work, not only to detect stars with large gaps, but to follow the evolution (in mass and size) of the outer disk in these stars where the inner disk is considerably evolved.

To summarize, the Hectochelle high-resolution spectra can explain the apparent contradictions found between the  $H\alpha$  EW and the presence of disks inferred from IR excesses. With the Hectochelle data, we can consistently explain 95% of the objects observed, with the remaining 5% corresponding mostly to stars with poor photometric and/or spectroscopic data.

## 4. Discussion

### 4.1. Accreting and non-accreting “transition objects”

One of the most interesting type of objects for the study of the processes leading to disk dissipation and planet formation are the “transition objects”. We define as “transition objects” the stars showing IR excess only at the longer wavelengths (typically, from the IRAC  $5.8\mu\text{m}$  band on; Paper III). Normally, these stars exhibit  $H\alpha$  EW (from low-resolution spectra) consistent with WTTS, and the discrepancy cannot be explained in terms of contamination by nearby stars, the emission from the globule (which can be important at 5.8, 8 and  $24\mu\text{m}$ ), nor because of photometric errors (Section 3.3). The lack of IR excess at shorter wavelengths suggests that important dust settling and/or grain growth have occurred in the

innermost part of these disks. Since accretion indicators point to very low or even no accretion, the presence of larger bodies (planets?) in the inner part of the disk, which might be responsible for the absence of gas flow (Lin & Papaloizou 1986; Bryden et al. 1999; D’Angelo et al. 2003; Quillen et al. 2004), cannot be ruled out. Planets have been invoked as a mechanism to clear up a gap in the disk, preventing in some cases accretion, as the inner disk cannot be replenished with gas coming from the outer disk (Forrest et al. 2004; D’Alessio et al. 2005). There are well-known cases of stars with non-detectable near-IR excesses and accretion (GM Tau and TW Hya are perhaps the most famous, see Calvet et al. 2002, Uchida et al. 2004) and with no accretion (CoKu Tau/4; Forrest et al. 2004). The lack of significant U band excess suggests very low accretion rates ( $\sim 10^{-9} - 10^{-10} M_{\odot}/\text{yr}$ ), so of high-resolution spectra are required in order to clarify the nature and presence of gas accretion in these objects.

Using Hectochelle in Tr 37, we can confirm the presence of both accreting and non-accreting “transition objects” (see Section 4.2 for a more detailed description of accretion rate limits in objects with no velocity wings). In Paper III, our definition of “transition objects” emphasized these objects with inner gaps and no accretion (small H $\alpha$  EW and no U excess). Given that Hectochelle has revealed the presence of both accreting and non-accreting “transition objects”, here we modify our definition to include all objects lacking near-IR excesses, independently of their accretion status. We have also revised the Spitzer photometry for this study, and although there are no significant changes, we have dropped from our list objects likely to be contaminated by either emission from the globule and/or nearby stars (these are the cases of 73-184 and 24-170). From the “transition object” list in Paper III, we did not observe two potential “transition objects”, 12-705 and 22-1569, which should be kept in mind for completeness and are good candidates for further study. Otherwise, the list stated here is the most complete and revised to the date. Note that, in any case, the number of “transition objects” is likely to be wavelength-dependent (Hartmann et al. 2005), and given that our data extend only to 24  $\mu\text{m}$ , we are not sensitive to objects with inner holes larger than a few AU, unless we are able to detect active accretion.

The stars 14-11, 13-52, and 13-566 are clearly not accreting, showing no velocity wings and profiles typical of WTTS despite of their large IR excess at wavelengths longer than 5.8 or 8  $\mu\text{m}$ . The stars 73-758, 21384350+5727270, 12-595, and 21392570+5729455 are most likely non-accreting as well, even though their spectra are noisy and might have some undetected higher velocity wings. On the other hand, the stars 13-1250 (K4.5, EW = -4/-2 Å), 21392541+5733202 (spectral type unknown, EW non-measurable), 24-515 (M0.5, EW non-measurable), 92-393 (M2, EW = -21/-34 Å), 21402192+5730054 (K6, EW = -4/-8 Å) and 13-819 (K5.5, EW = -6/-10 Å) show H $\alpha$  profiles characteristic of accretion, in spite of their lack of near-IR excess. It is worth to mention that all the accreting “transition objects”

(except for 92-393<sup>4</sup>) have very small H $\alpha$  EW, comparable to WTTS, or in the limit between CTTS and WTTS (non-measurable in the cases of 21392541+5733202 and 24-515 due to difficulties subtracting the background component when the velocity wings are so small). The small EW is suggestive of a very small accretion rate, what we can corroborate based on the U band observations presented in Paper II. The only stars with detectable U band excess are 13-1250 and 13-819, which were observed in two different campaigns. For 13-1250 (which may also have a very small excess over the photosphere), one of the observations results in non-significant U band excess, and the other observation reveals a small excess (in the limit of detectability) that could be related to an accretion rate around  $10^{-9} M_{\odot}/\text{yr}$ . For 13-819, the accretion rate varies from  $4 \times 10^{-10}$  to  $2 \times 10^{-9} M_{\odot}/\text{yr}$ , confirming our predictions of very low accretion rates.

Taking into account the number of bona fide “transition objects” ( $\sim 10\%$  of the stars with disks), and comparing to the number of disks expected to have disappeared within the past 3 Myr (considering that regions aged  $\sim 1$  Myr have  $\sim 80\%$  of disks, and that the 4 Myr-old Tr 37 has only  $\sim 45\%$  disk fraction, and assuming a constant rate of disk dissipation), we estimated a short life for these disks with inner gaps (from few times  $\sim 10^5$  yr to less than 1 Myr; Paper III). Since here we find that accretion is present in only about half of the “transition objects”, the same argument predicts an even shorter timescale for stopping accretion or bringing it down to undetectable levels, once a gap has been opened in the inner disk. On the other hand, the timescales for the opening of the gap remain uncertain, given the lack of detailed studies of “transition objects” in younger and older clusters. At this point, it is not possible to determine whether the opening of the gap occurs rapidly in a normal CTTS-like disk, or whether it is a longer process starting with the decrease in near-IR emission with age. In Paper III we observed that more than 95% of the disks are below the median SED in Taurus, and that this difference is more striking at shorter wavelengths. Tr 37 presents as well some disks showing a remarkable “kink” in their SEDs, or an abrupt change in the SED slope occurring at about  $8\mu\text{m}$  (see the cases of 73-472 and 11-2031 among others) that could be suggestive of a smooth evolution into the “transition object” class. Nevertheless, detailed studies of other populations are required to prove the timescales of gap opening.

Even though the fraction of “transition objects” is small, it is too large to be explained by the presence of a close stellar (or substellar) companion (which would be otherwise a plausible mechanism to explain the inner gaps without requiring disk evolution), taking

---

<sup>4</sup>This star has an spectral type M2. According to White & Basri 2003, stars of spectral types later than M2 may have chromospheric values of H $\alpha$  up to 20Å, so this would place 92-393 in the limit between CTTS and WTTS as well

into account the low close-in (few AU) binary fractions for low-mass stars (Mathieu 1994; Lada 2006). Note that none of the “transition objects” is found to be neither SB2 nor SB1. Photoevaporation of the inner disk by the central star would be another method to produce inner gaps without involving dust coagulation and/or planet formation (Clarke et al. 2001). Photoevaporation could remove the gaseous and dusty component of the inner disk in timescales comparable to the disk dissipation, producing a very brief ( $\sim 10^5$  yr) phase during which the inner disk is not present, before the outer disk is dissipated. The size of the resulting inner gap depends on the UV flux emitted by the star, so larger gaps are expected for earlier-type stars (Alexander et al. 2006a,b). Further observations, oriented at the detection of photoevaporation and photodissociation of gas in the outer (still optically thick) disk would be required in order to determine if photoevaporation may be involved in the disk dissipation.

The presence of gas accretion in half of the “transition objects” may suggest grain growth and/or planet formation rather than photoevaporation as the main cause for the near-IR gaps, as significant amounts of gas need to remain in the disk and/or to flow through it. Grain growth to large sizes would result in a decrease of the opacity at near- and mid-IR wavelengths, as we observe in about 90% of the disks in Tr 37 (Paper III), and grain growth to large (m or km) sizes would probably not affect the gas flow in the disk. The formation of one or more planets would create a gap as well, and depending on the planet and disk masses, slow accretion could occur for some time through the gap, being able to reproduce both accreting and non-accreting “transitional disks” (Lin & Papaloizou 1986; Bryden et al. 2000; D’Angelo et al. 2003; Quillen et al. 2004).

Considering the limited spectral type range covered in this study, we do not see any correlation between the spectral type and the presence and/or characteristics of the gaps. The “transition objects” we find in Tr 37 have spectral types ranging from K4 to M2, which is the range containing most (96%) of the studied objects. Despite the low number of “transition objects” observed, we do not observe any tendency of “transition objects” to have spectral type M, as pointed out by McCabe et al. (2006). Note that the McCabe sample contains more late-M stars than ours (which goes down to M2 stars), but nearly 80% of the objects observed by them are comparable to ours in spectral type. Another point to be considered is that the sample in McCabe et al. (2006) is younger ( $\sim 1$  Myr) than ours, which is an important fact to be taken into account for timescale estimates in the future. The spectral type distribution of our “transition objects” is consistent with random sampling in our population. We do not see either any correlation between SEDs and spectral types, in the sense that most of these objects show photospheric colors at wavelength shorter than  $\lambda \sim 6 \mu\text{m}$  independently of their spectral types, and the excesses at or beyond  $6\mu\text{m}$  do not show any significant dependence with spectral type. Since our Spitzer study is complete



only down to  $8\ \mu\text{m}$  (the  $24\ \mu\text{m}$  detection limit only covers photosphere emission from B-type stars, and it is about 1-2 orders of magnitude over the typical photosphere of a TTS; Paper III), the detection of gaps larger than  $\sim 5$  AU around low-mass stars is difficult or impossible with this set of data, unless the outer disks are very luminous or we can infer the presence of an outer undetected disk because of the presence of accretion. Therefore, our study may be missing some non-accreting “transition objects” with larger gaps. Note that the generalized sensitivity limitations for detecting large gaps and/or “debris disks” around stars with spectral types later than A may explain part of the bias towards finding larger gaps around more massive stars. Here, the only case of a low-mass star with a confirmed large gap is 13-819, which has no excess even at  $8\ \mu\text{m}$ . It is confirmed to have some outer disk due to its accretion, detectable via both  $\text{H}\alpha$  emission and U band excess. Given its spectral type (K5.5), similar to other “transition objects” (like 13-566, 21402192+5730054), we do not find any correlation between spectral type and size of the gap. Although the limitation both in number of objects and in the reduced spectral type range covered by these observations must be taken into account, these data suggest that photoevaporation alone is probably not able to reproduce the set of observed “transition objects”, and additional mechanisms as grain growth to large (planetesimal) sizes and/or planet formation must be invoked.

Among the potential “transition objects” with larger gaps (even though they must be regarded with care due to the lack of  $24\ \mu\text{m}$  data to confirm the presence of a disk), we would like to mention the case of several stars showing a small excess at  $8\ \mu\text{m}$  only (typically, 7-10 sigma over the photospheric emission, Paper III) and no broad  $\text{H}\alpha$  line emission. The lack of  $24\ \mu\text{m}$  counterparts suggest that emission at these wavelength is below our detection limit (keeping in mind that our detection limit is one to two orders of magnitude above the photospheric emission of low-mass stars), as it happens in other stars with normal-looking but relatively flat accretion disks (see 13-1891 and 12-1010 among others). The star 13-350 (M1) is one of these cases, having a very small excess at  $5.8\ \mu\text{m}$ , in addition to a  $\sim 10$  sigma excess at  $8\ \mu\text{m}$ , which makes it a good candidate to be another non-accreting “transition object”. Other stars with excesses only at  $8\ \mu\text{m}$  are 14-222 (K7), 14-2148 (M1.5), 54-1613 (K5), and 92-1162 (M2). Both 14-222 and 54-1613 have uncertain very small U band excesses. As mentioned in Paper III, the fact that this kind of objects is nearly absent from the older cluster NGC 7160, suggests that at least part of them are true detections of “transition objects” and not photometry errors. Further followup of these objects at longer wavelengths and with improved sensitivity would be recommendable, in order to estimate the fraction (and therefore, timescales) of “transition objects” more accurately.

## 4.2. Accretion rate evolution

Inspecting the  $H\alpha$  profiles, we can complete our knowledge about the accretion rates that we obtained from U band photometry (Gullbring et al. 1998). The accretion rate calculations are described in detail in Paper II. There, we measured the excess of U band luminosity over the photospheric level, related to the accretion luminosity by the prescription in Gullbring et al. (1998). U band excesses corresponding to accretion rates below  $10^{-9} M_{\odot}/\text{yr}$  are in general difficult to detect (based on our U band sensitivity for K7-M2 stars; Paper II), but the presence of  $H\alpha$  high velocity wings can be used as a direct proof of accretion or no accretion even in those cases. For objects with velocity wings broader than 200 km/s and no detectable U excess, we assign  $10^{-9} M_{\odot}/\text{yr}$  as an upper limit to the accretion rate. We define as non-accretors all these objects showing no U excess and/or no U detection (our U photometry detects photospheric U band emission only down to a K6-K7 star, see Paper II) and no velocity wings broader than  $\sim 200$  km/s (White & Basri 2003; Natta et al. 2004). According to the models by Muzerolle et al. (2003), accretion rates under  $10^{-12} M_{\odot}/\text{yr}$  do not result in significant line broadening, so these objects would have accretion rates below  $10^{-12} M_{\odot}/\text{yr}$ , if any. In the cases where no excess from a disk is detected at any wavelength, the accretion rate is likely to be zero or negligible. Whenever no U band photometry is available, we base the accretion/non accretion criterion on the presence of velocity wings. In case of any doubts about the profiles, we prefer to be conservative, assigning an upper limit to the accretion rate of  $\sim 10^{-9} M_{\odot}/\text{yr}$ . Table 2 contains the accretion rates from Paper II, completed with the new upper limits for the sure and probable members.

Since the  $H\alpha$  observations complete our information about accretion processes in  $\sim 80\%$  of all the stars, we have revisited the accretion vs. age diagram described in Paper II, including all the new upper limits (Figure 11). Compared to the evolution of a viscous disk (Hartmann et al. 1998; Muzerolle et al. 2000), we find better evidence of the decrease of accretion rate with time (using ages derived from the dereddened V vs. V-I diagrams, which proved to be less affected by observational errors than the HR diagram, and the Siess et al. 2000 isochrones; Paper II). The fraction of stars with accretion rates under  $10^{-9} M_{\odot}/\text{yr}$  is significantly larger than in younger clusters, and we can set an upper limit to the median accretion rate of around  $1 \times 10^{-9} M_{\odot}/\text{yr}$  (including the  $10^{-9} M_{\odot}/\text{yr}$  upper limits in the calculation). The average rate is  $9 \times 10^{-9} M_{\odot}/\text{yr}$  (including the  $10^{-9} M_{\odot}/\text{yr}$  upper limits), slightly lower than the  $2 \times 10^{-8} M_{\odot}/\text{yr}$  average obtained with the U band photometry alone, and slightly lower than the Taurus average ( $10^{-8} M_{\odot}/\text{yr}$ ). However, given that the standard deviation is around  $2.3 \times 10^{-8} M_{\odot}/\text{yr}$  because it depends mostly on a few very strong accretors, the median rate is probably more significant (note that we have excluded from these calculations the G-type stars, which show systematically higher accretion rates). The IR excess in Tr 37, which are systematically lower than in Taurus (especially at shorter

wavelengths, see Paper III), the higher number of very slow accretors in Tr 37 compared to Taurus, and the fact that accretion rates are in general below the Taurus average suggest that the evolution of the dust is somehow parallel to the gas and accretion evolution. The fact that the “transitional disks” with inner IR gaps present accretion rates never larger than  $10^{-9} \text{ M}_{\odot}/\text{yr}$ , and consistent with  $\dot{M} < 10^{-9} \text{ M}_{\odot}/\text{yr}$  or even zero (Class III-like) accretion in about half of the cases, seems to indicate a correlation between dust and gas evolution as well.

Following Muzerolle et al. (2003), Natta et al. (2004), and Calvet et al. (2004), we search for a correlation between mass and accretion rate. As we did in Paper II, we derived masses directly from the extinction-corrected V vs. V-I diagram (see Table 2 for the individual values of age and mass). Even though most of our stars are roughly the same mass, we can see a slight evidence of a  $\dot{M} \propto M^a$  trend in Figure 12. Comparing to the sample in Calvet et al. (2004) and Natta et al. (2004), we find that our stars are consistent with their samples, although our reduced differences in  $M$  and in accretion rates here does not make a  $\dot{M} \propto M^2$  relation evident. If we take into account the age differences (even though the ages for G-type stars are highly uncertain), we find that the stars belonging to the globule population (which are  $\sim 1$  Myr old instead of 4 Myr, Paper II) show a similar trend, but with systematically higher mass accretion rates, as we would expect from the viscous disk evolutionary models (Hartmann et al. 1998; Muzerolle et al. 2000; Figure 11).

### 4.3. Rotation rates of accreting and non-accreting stars

The high-resolution spectra allow us to face the question concerning the way stars are released from their inner disks during the processes of planet formation and disk evolution. This could have important consequences on the evolution of the disk and the angular momentum of the star. There is still a large controversy about the way accreting stars are connected to their disks, and about the combined effects of contraction, accretion and winds on the angular momentum of the star (Bouvier et al. 1993; Edwards et al. 1993; Stassun et al. 1999; Rhode et al. 2001; Küker et al. 2003). One interpretation suggests that the presence of an accreting disk would lock the star, preventing it from speeding up as it contracts and accretes (Bouvier et al. 1993; Shu et al. 1994; Choi and Herbst 1996; Herbst et al. 2002; Hartmann 2002). Other observations suggest that disk accretion and stellar contraction may affect the stellar rotation differently, resulting in rotational periods that do not change with time (Stassun et al. 2001). Some observations could be also consistent with a picture where the star-disk connection may not have any appreciable effects on the rotation of the star, so the observed differences would be mostly related to initial conditions rather than to age or

evolutionary stage (Stassun et al. 2001). It has been also suggested that the effects of disk locking may be time-dependent, so disk locking could start only some time after the formation of the Class II system, or conversely, it could disappear with age as the accretion rates drop down while the disk evolves (Hartmann 2002). Nevertheless, the time-dependence of disk locking is highly uncertain, given the lack of rotational studies of large populations with different ages. At the present moment, there is no clear answer, as different studies result in different conclusions, and it is not known yet whether some historical problems identifying accretion processes and/or the presence of disks may be responsible for the variety of results (Sicilia-Aguilar et al. 2005), or whether this is a physical difference resulting from different ages, initial conditions, environment or evolutionary stages.

Here, we investigate the possible correlation between stellar rotation ( $V_{\text{ sini}}$ ) and the presence of accretion and/or accretion disks. Tr 37 is a specially interesting cluster to study the effect on rotation of disk locking because it is older than previously studied young clusters, and younger than mid-aged stars, which are no longer accreting. We use the broad  $H\alpha$  emission and the IR excesses (based on the [3.6]-[4.5] and [3.6]-[5.8] IRAC colors, see Paper III) to define the presence of ongoing accretion and of an inner disk, respectively (for more detail in the correlation of accretion and IR excesses, see Section 3.3). We have constructed histograms for the rotational velocities  $V_{\text{ sini}}$  for the stars with and without signatures of accretion and inner disk, separating them in 10 km/s bins (in order to minimize the errors derived from the fiber tilts, Section 2). Considering only the stars with high signal-to-noise and good correlations, as well as good IRAC/Spitzer photometry, our sample is reduced to 34 stars with broad  $H\alpha$  vs. 46 stars with narrow  $H\alpha$ , 32 stars with [3.6]-[4.5] excess vs. 29 stars without this excess, and 22 stars with [3.6]-[5.8] excess vs. 39 stars without [3.6]-[5.8] excess, which may mean low-number statistics. The different histograms are shown in Figure 13. From the comparison, we do not find any significant differences in the rotation of CTTS and WTTS stars according to any of these three definitions. Given the good correlation of IR excess and broad  $H\alpha$  profiles (Section 3.3), except for the few accreting “transition objects”, all the histograms are very similar. Even though these results are based on low-number statistics, the lack of significant differences could suggest that either disk locking is not an important mechanism regulating the rotation of the stars, or it is only important at earlier stages, when accretion rates are higher and dust settling/grain growth is not so widely present.

Comparing with our previous study of the Orion Nebula Cluster (Sicilia-Aguilar et al. 2005) we find relevant differences in the rotation of WTTS (see Figure 13) in the two regions. The fraction of WTTS with high rotational velocities is significantly higher in the ONC than in Tr 37, and the distribution of rotational velocities of CTTS and WTTS in the ONC are clearly different (Sicilia-Aguilar et al. 2005). The ONC and Tr 37 differ in age ( $\sim 1$  Myr

versus  $\sim 4$  Myr respectively), disk fraction ( $\sim 80\%$  versus  $\sim 45\%$ ) and environment (the ONC being much denser, with more massive stars, more embedded in the original nebula, and more populous than Tr 37), so it is not clear that their star formation and disk evolution histories can be simply compared. Even though the differences in rotation between Tr 37 and the ONC may suggest some degree of rotational evolution during the first million years of the life of a star, the observed variations may just show a dependence on initial and/or environmental conditions, as suggested by Stassun et al. (2001).

## 5. Conclusions

We presented a study of the accretion processes occurring in the 4 Myr-old cluster Tr 37, using the high-resolution spectrograph Hectochelle in the MMT telescope, to observe the  $H\alpha$  order. Observing a total of 460 stars, we confirmed the membership and accretion properties of 144 previously known members, and we found a total of 26 new members and probable members, according to their  $H\alpha$  emission and to their radial velocities. We use  $H\alpha$  as a powerful sign of accretion (characterized by asymmetric profiles and broad velocity wings), enabling us to detect stars with accretion rates well below  $10^{-9} M_{\odot}/\text{yr}$  and up to  $10^{-12} M_{\odot}/\text{yr}$ , which are below the detection limits of U band surveys. This way, we are able to set limits to accretion to a large number of stars in the cluster, finding that the average accretion rate is lower than in younger regions (i.e. Taurus), being of the order of  $9 \times 10^{-9} M_{\odot}/\text{yr}$ . Given the similarities between the decrease in IR excesses observed in Tr 37 with respect to Taurus, and the decrease in accretion rates, gas evolution seem to occur somehow parallel to the evolution of the dust grains and the structure of the disk.

We find that “transition objects”, or stars with inner gaps in their disks (seen as objects with no IR excess at wavelength shorter than  $\sim 6 \mu\text{m}$ ) show either no accretion ( $< 10^{-12} M_{\odot}/\text{yr}$ ) or are consistent with extremely low accretion rates, mostly undetectable from U band photometry (which sets an upper limit of  $10^{-9} M_{\odot}/\text{yr}$ ). The “transition objects” represent about 10% of the total number of disks observed in Tr 37, and about half of them do not show any evidence of accretion. The number of “transition objects” observed here is large than in other regions, although this study is more complete than others since it includes observations up to  $24 \mu\text{m}$  and high-resolution spectra, so we are able to identify some objects looking as intermediate stages between class II and class III as “transition objects”. Additionally, accretion rates seem much lower (or undetectable) in the potential disks with larger gaps, even though we find 1 case of accretion in a disk with a large inner gap (presumably  $> 5\text{-}10$  AU). The decrease and termination of the accretion processes as the inner disk clears up/agglomerates suggest that the evolution of dust and gas occurs in

a parallel way, and that mass accretion may cease shortly after the formation of these inner disk gaps. Therefore, these objects are a key to the intermediate stage between CTTS and WTTS, in which accretion processes are terminating and important planet formation may be taking place.

Even though the sample of “transition objects” is limited in number and in spectral type coverage, the fact that half of the “transition objects” are accreting may suggest grain growth and planetesimal (or even planet) formation as the cause for inner gaps in disks, at least in part of the objects. We do not observe any differences in the size of the gap according to the spectral type, and the presence of 1 confirmed and several probable disks with large gaps seem to suggest that stars with the same spectral type can have inner holes of different sizes. These observations would suggest that grain growth/settling is responsible for the opening of inner gaps, rather than photoevaporation alone. Observations at longer wavelengths would be advisable in order to confirm the larger gaps and the presence of rims and walls, and UV line observations could be used to determine the presence of photoevaporation in the rim of the outer disk of “transition objects”.

Finally, we obtain the rotational velocities for about 75% of the stars, finding no significant differences between the rotation of accreting and non-accreting stars. Therefore, disk locking is either not relevant at the age of 4 Myr, or it is dependent of the environment, or the differences observed in other regions account rather for different initial conditions than for the evolutionary stage.

We want to acknowledge J. Muzerolle, S. Mohanty and B. Merín for the interesting comments and discussion. We also want to thank the anonymous referee for the detailed review of our paper and useful comments. This publication makes use of data products from the Two Micron All Sky Survey, which is a joint project of the University of Massachusetts and the Infrared Processing and Analysis Center/California Institute of Technology, funded by the National Aeronautics and Space Administration and the National Science Foundation. This work made use of the VizieR Astronomical Database.

## A. APPENDIX: The star 13-277

A special case that deserves attention is the star 13-277. It is classified as a late G/early K star (the spectral type is uncertain due to high veiling), and it has an extremely bright disk, plus extremely high luminosity for a late-type star ( $L \sim 26 L_{\odot}$ ). Its accretion rate, although uncertain, is much higher than the average accretion rate in Tr 37, being approximately  $\sim 3 \times 10^{-7} M_{\odot}/\text{yr}$  according to its 10%  $H\alpha$  EW (see Natta et al. 2004), and maybe up to  $10^{-5}$

$M_{\odot}/\text{yr}$  (depending on the actual spectral type) calculated from the U band excess. It is by far the fastest rotator in the cluster ( $V\sin i \sim 52$  km/s, the next fastest rotator has  $V\sin i \sim 28$  km/s). Its radial velocity is slightly off-cluster (with a deviation slightly higher than  $2\sigma$ ), but this is most likely due to the difficulties obtaining accurate radial velocities when the lines are very broadened by rotation.

This star could be the object named  $G\mu$  Cep and noted as a long-period variable by Morgenroth (1939). There is an offset of about 1 arcmin in declination between 13-277 and  $G\mu$  Cep, but the position cited by Morgenroth (1939) does not correspond to any other object. In that case, the photometry from the Sonneberg Observatory reveals variations up to 2 magnitudes, although it does not cite any kind of periodicity nor timescale for the star. At the present time, 13-277 would be about its maximum magnitude cited in Morgenroth (1939). Given that high accretion, extreme brightness, and fast rotation are some of the characteristics of FU Ori and for EX Ori objects (Hartmann & Kenyon 1996; Herbig et al. 2003; Vittone & Errico 2005), and that its disk is comparable to the brightest CTTS disk known (GW Ori; Mathieu et al. 1995), we are planning an optical and radio followup of this object in order to determine its true nature.

## REFERENCES

- Alexander, R.C., Clarke, C.J., Pringle, J.E., 2006a, MNRAS in press
- Alexander, R.C., Clarke, C.J., Pringle, J.E., 2006b, MNRAS in press
- André, Ph., & Montmerle, T., 1994, ApJ, 420, 837
- Appenzeller, I., & Mundt, R., 1998, AARV, 1, 291
- Armitage, Ph., Clarke, C., Palla, F., 2003, MNRAS, 342, 1139
- Bergin, E., Calvet, N., Sitko, M., and 9 more coauthors, 2004, ApJ, 614, L133
- Bertout, C., 1989, ARA&A, 27, 351
- Bonnell, I. A., Smith, K. W., Meyer, M. R., Tout, C. A., Folha, D. F. M., & Emerson, J. P. 1998, MNRAS, 299, 1013
- Bouvier, J., Cabrit, S., Fernández, M., Martín, E.L., Matthews, J.M., AA, 272. 176
- Bryden, G, Rozyczka, M., Lin, D., Bodenheimer, P., 2000, 540, 1091
- Cabrit, S., Edwards, S., Strom, S., Strom, K., 1990, ApJ, 354, 687

- Calvet, N. & Hartmann, L. W. 1992, ApJ, 386, 239
- Calvet, N. & Gullbring, E., 1998, ApJ, 509,802
- Calvet, N., D’Alessio, P., Hartmann, L., Wilner, D., Walsh, A. & Sitko, M., 2002, ApJ, 568, 1008
- Calvet, N., Muzerolle, J., Briceño, C., Hernández, J., Hartmann, L., Saucedo, J. L., & Gordon, K. D. 2004, AJ, 128, 1294
- Calvet, N., Briceño, C., Hernández, J., Hoyer, S., Hartmann, L., Sicilia-Aguilar, A., Megeath, S.T., D’Alessio, P., 2005, AJ139, 935
- Carpenter, J., Snell, R., Schloerb, F.P., 1990, ApJ, 362, 147
- Choi, P.I., & Herbst, W., 1996, AJ, 111, 283
- Clarke, C., Gendrin, A., & Sotomayor, M., 2001, MNRAS 328, 485
- Contreras, M.E., Sicilia-Aguilar, A., Muzerolle, J., Calvet, N., Berlind, P., Hartmann, L. 2002, AJ, 124, 1585
- D’Alessio, P., Hartmann, L., Calvet, N., Franco-Hernández, R., and 10 more coauthors, 2005, ApJ, 621, 461
- D’Angelo, G., Henning, Th., & Kley, W., 2003, ApJ, 599, 548
- Edwards, S., Strom, S., Hartigan, P., Strom, K., Hillenbrand, L., Herbst, W., Attridge, J., Merrill, K., Probst, R., Gatley, I., 1993, AJ, 106, 372
- Fabricant, D.G. et al 2004, Proc SPIE in press
- Forrest, W.J., Sargent, B., Furlan, E., & 18 more coauthors, 2004, ApJS, 154, 443
- Fűrész, G., et al., 2006, ApJ in press
- Gregorio-Hetem, J., & Hetem, A. Jr., 2002, MNRAS, 336, 197
- Gullbring, E., Hartmann, L., Briceño, C., Calvet, N., 1998, ApJ 492, 323
- Haisch, K., Lada, E., & Lada, C., 2001, ApJ, 553,153
- Hartigan, P., Hartmann, L., Kenyon, S., Strom, S., & Skrutskie, M., 1990, ApJ, 354, 25
- Hartmann, L., Hewett, R., Stahler, S., Mathieu, R., 1986, ApJ, 309, 275



- Hartmann, L., & Kenyon, S., 1996, ARAA, 34, 207
- Hartmann, L.: Accretion Processes in Star Formation, Cambridge University Press, 1998.
- Hartmann, L., Calvet, N., Gullbring, E. & D'Alessio, P, 1998, ApJ, 495, 385
- Hartmann, L., 2002, ApJ, 566, 29
- Hartmann, L., 2003, ApJ, 585, 398
- Herbig, G.H., 1998, ApJ, 497, 736
- Herbst, W., Bailer-Jones, C., Mundt, R., Meisenheimer, K., Wackermann, R., 2002, AA, 396, 513
- Herbst, W., Herbst, D.K., Grossman, E.J., & Weinstein, D., 1994, AJ, 108, 1906
- Kenyon, S.J. & Hartmann, L., 1995, ApJS , 101, 117
- Küker, M., Henning, Th., Rüdiger, G., 2003, ApJ, 589, 397
- Kurtz, M.J., Mink, D.J., Wyatt, W.F., Fabricant, D.G., Torres, G., Kriss, G., and Tonry, J.L. 1992, in Astronomical Data Analysis Software and Systems I, ASP Conf. Ser., Vol. 25, eds. D.M. Worrall, C. Biemesderfer, and J. Barnes, 432
- Lada, C.J., 1987, IAUS, 115, 1L
- Lada, C.J., Muench, A.A., Haisch, K.E., Lada, E.A., Alves, J.F., Tollestrup, E.V. & Willner, S.P., 2000, AJ, 120, 3162
- Lin, D.N.C., & Papaloizou, J., 1986, ApJ, 309, 846
- Littlefair, S., Naylor, T., Harries, T., Retter, A., O'Toole, S., 2004, MNRAS 347, 937
- Mathieu, R., Adams, F., Fuller, G., et al. 1995, AJ 109, 265
- Morgenroth, O., 1939, Astron. Nach. 268, 273
- Muzerolle, J., & Hartmann, L., & Calvet, N., 1998a, AJ, 116, 455
- Muzerolle, J., Calvet, N. & Hartmann, L., 1998b, ApJ, 492, 743
- Muzerolle, J., Calvet, N., Briceño, C., Hartmann, L. & Hillenbrand, L., 2000, ApJ, 535, L47
- Muzerolle, J., Calvet, N. & Hartmann, L., 2001, ApJ, 550, 944

- Muzerolle, J., Hillenbrand, L., Calvet, N., Briceño, C., Hartmann, L., 2003, ApJ, 592, 266
- Natta, A., Testi, L., Muzerolle, J., Randich, S., Comeron, F., & Persi, P., 2004, A&A, 424, 603
- Patel, N.A. , Goldsmith, P.F., Snell, R.L., Hezel, T. & Xie, T., 1995, ApJ , 447, 721
- Patel, N.A., Goldsmith, P.F., Heyer, M.H. & Snell, R.L., 1998, ApJ , 507, 241
- Platais, I., Kozhurina-Platais, V., van Leeuwen, F., 1998, AJ, 116, 2423
- Podosek, F.A. & Cassen, P., 1994, Meteoritics 29, 6-25
- Quillen, A., Blackman, E., Frank, A., Varniere, P., 2004, ApJ, 612, L137
- Randich, S., Pallavicini, R., Meola, G., Stauffer, J.R., & Balachandran, S.C., 2001, A&A, 372, 862
- Reipurth, B., Pedrosa, A., Lago, M.T.V.T., 1996., AASS, 120, 229
- Rhode, K., Herbst, W. & Mathieu, R., 2001, AJ, 122, 3258
- Shu, F., Najita, J., Ostriker, E., Wilkin, F., Ruden, S., & Lizano, S., 1994, ApJ, 429, 781
- Sicilia-Aguilar, A., Hartmann, L., Briceño, C., Muzerolle, J., & Calvet, N., 2004, AJ128, 805, Paper I
- Sicilia-Aguilar, A., Hartmann, L., Szentgyorgyi, A., Roll, J., Conroy, M., Calvet, N., Fabricant, D., & Hernández, J., 2005, AJ, 129, 363
- Sicilia-Aguilar, A., Hartmann, L., Hernández, J., Briceño, C., Calvet, N., 2005, AJ130, 188, Paper II
- Sicilia-Aguilar, A., Hartmann, L., Calvet, N., Megeath, S.T., Muzerolle, J., Allen, L., D'Alessio, P., Merín, B., Stauffer, J., Young, E., Lada, C., 2006, ApJ 638, 897, Paper III
- Siess, L., Dufour, E. & Forestini, M. 2000 A&A , 358, 593S
- Skrutskie, M., Dutkevitch, D., Strom, S., Edwards, S., & Strom, K., 1990, AJ, 99, 1187
- Spitzer, L., 1984, Sci. 225, 466
- Stassun, K., Mathieu, R., Vrba, T., Henden, A., 2001, AJ, 121, 1003

- Stassun, K., Mathieu, R., Mazeh, T., Vrba, T., 1999, AJ, 117, 2941
- Strom, K., Wilkin, F., Strom, S., & Seaman, R., 1989, AJ, 98, 1444
- Szentgyorgyi, A. H., Cheimets, P., Eng, R., Fabricant, D. G., Geary, J. C., Hartmann, L.,  
Pieri, M. R., & Roll, J. B., 1998, Proc. SPIE, 3355, 242
- Tonry, J., & Davis, M., 1979, AJ 84, 1511
- Uchida, K. I., et al. 2004, ApJS, 154, 439
- Vittone, A., & Errico, L., 2005, Mem. S.A.It. 76, 320
- White, R., & Basri, G., 2003, ApJ, 582, 1109

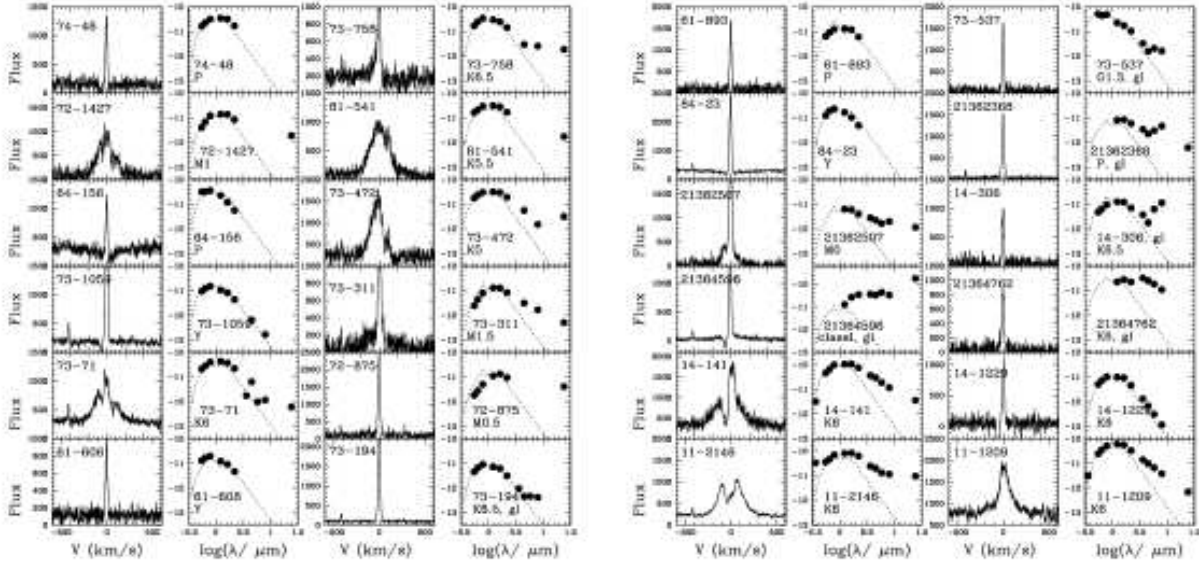


Fig. 1.—  $H\alpha$  profiles and SEDs of the observed members and potential members, showing the optical UVRI and JHK 2MASS fluxes (Paper I, II), IRAC (3.6, 4.5, 5.8, 8.0  $\mu\text{m}$ ; Paper III) and MIPS(24 $\mu\text{m}$ ; Paper III) data. A photosphere (Kenyon & Hartmann 1995) for the given spectral type is displayed in each case to clarify the presence of an IR excess. The nebular emission was successfully subtracted from the broad  $H\alpha$  profiles with good S/N. Narrow  $H\alpha$  lines, as well as some low S/N broad profiles, are contaminated by the nebular emission. The units of the fluxes are counts (non-calibrated) for the  $H\alpha$  lines, and  $\log(\lambda F_\lambda)$  in  $\text{erg cm}^{-2} \text{s}^{-1}$  for the SEDs. The label “gl” marks the stars embedded in the Tr 37 globule, which may have large errors in the Spitzer photometry (mostly in the 5.8 and 8.0  $\mu\text{m}$  IRAC bands).

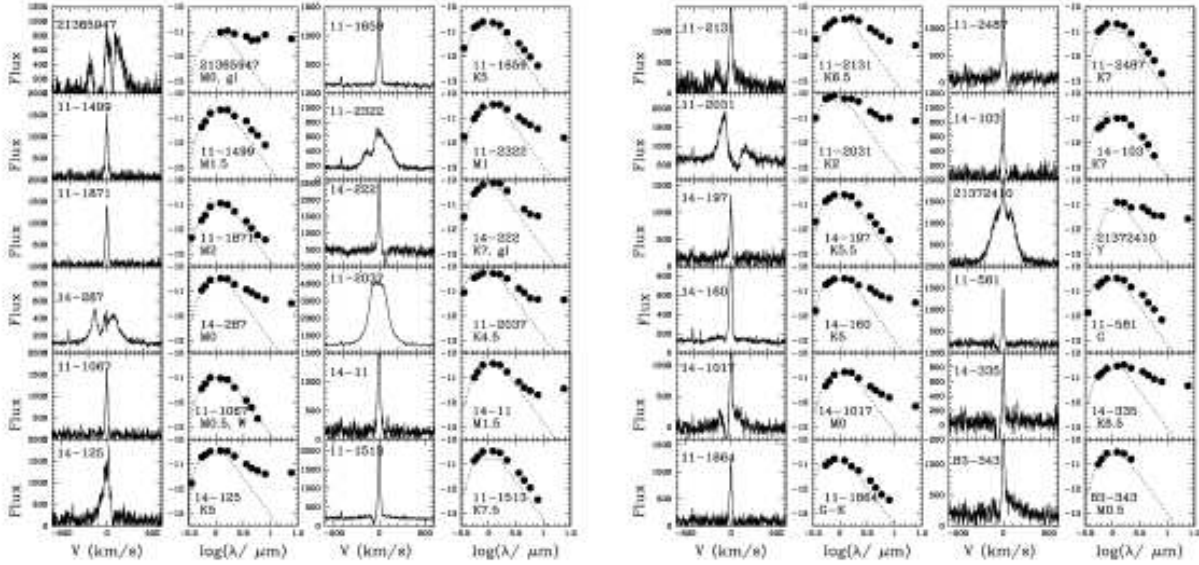


Fig. 2.—  $H\alpha$  profiles and SEDs of the observed members and potential members, showing the optical UVRI and JHK 2MASS fluxes (Paper I, II), IRAC (3.6, 4.5, 5.8, 8.0  $\mu\text{m}$ ; Paper III) and MIPS(24 $\mu\text{m}$ ; Paper III) data. A photosphere (Kenyon & Hartmann 1995) for the given spectral type is displayed in each case to clarify the presence of an IR excess. The nebular emission was successfully subtracted from the broad  $H\alpha$  profiles with good S/N. Narrow  $H\alpha$  lines, as well as some low S/N broad profiles, are contaminated by the nebular emission. The units of the fluxes are counts (non-calibrated) for the  $H\alpha$  lines, and  $\log(\lambda F_\lambda)$  in  $\text{erg cm}^{-2} \text{s}^{-1}$  for the SEDs (continued).

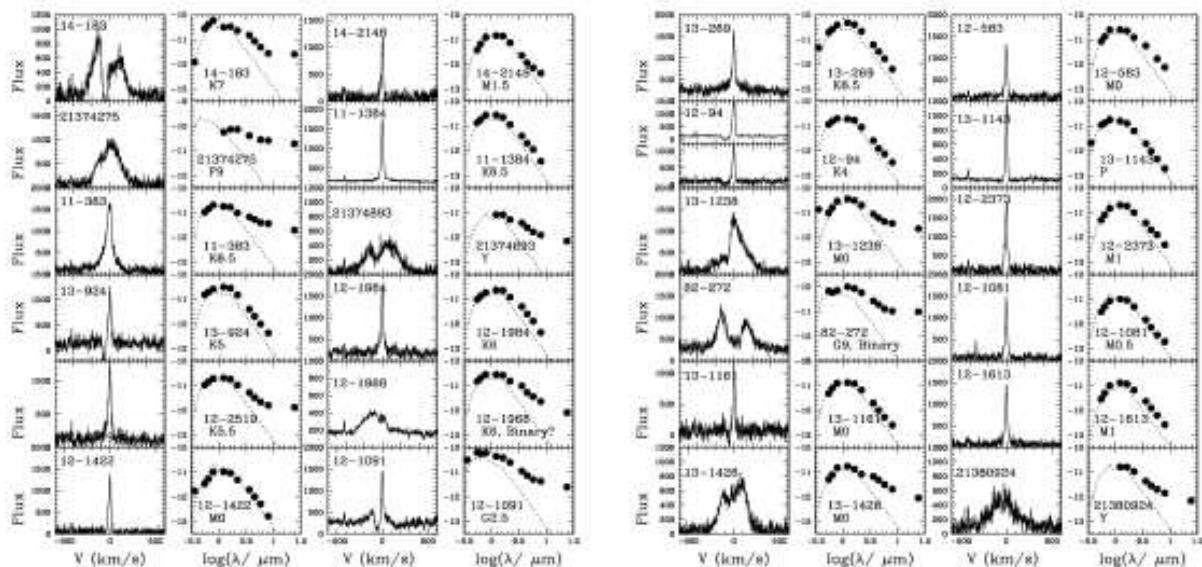


Fig. 3.—  $H\alpha$  profiles and SEDs of the observed members and potential members, showing the optical UVRI and JHK 2MASS fluxes (Paper I, II), IRAC (3.6, 4.5, 5.8, 8.0  $\mu\text{m}$ ; Paper III) and MIPS(24 $\mu\text{m}$ ; Paper III) data. A photosphere (Kenyon & Hartmann 1995) for the given spectral type is displayed in each case to clarify the presence of an IR excess. The nebular emission was successfully subtracted from the broad  $H\alpha$  profiles with good S/N. Narrow  $H\alpha$  lines, as well as some low S/N broad profiles, are contaminated by the nebular emission. The units of the fluxes are counts (non-calibrated) for the  $H\alpha$  lines, and  $\log(\lambda F_\lambda)$  in  $\text{erg cm}^{-2} \text{s}^{-1}$  for the SEDs (continued).

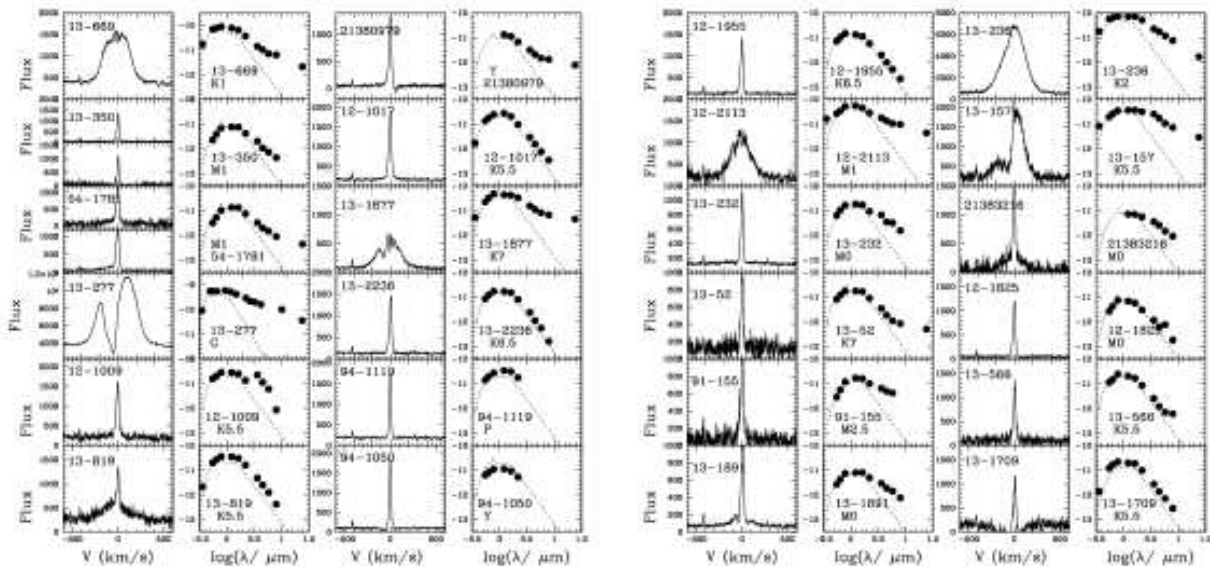


Fig. 4.—  $H\alpha$  profiles and SEDs of the observed members and potential members, showing the optical UVR-I and JHK 2MASS fluxes (Paper I, II), IRAC (3.6, 4.5, 5.8, 8.0  $\mu\text{m}$ ; Paper III) and MIPS(24 $\mu\text{m}$ , 70  $\mu$  only for 13-277; Paper III) data. A photosphere (Kenyon & Hartmann 1995) for the given spectral type is displayed in each case to clarify the presence of an IR excess. The nebular emission was successfully subtracted from the broad  $H\alpha$  profiles with good S/N. Narrow  $H\alpha$  lines, as well as some low S/N broad profiles, are contaminated by the nebular emission. The units of the fluxes are counts (non-calibrated) for the  $H\alpha$  lines, and  $\log(\lambda F_\lambda)$  in  $\text{erg cm}^{-2} \text{s}^{-1}$  for the SEDs (continued).

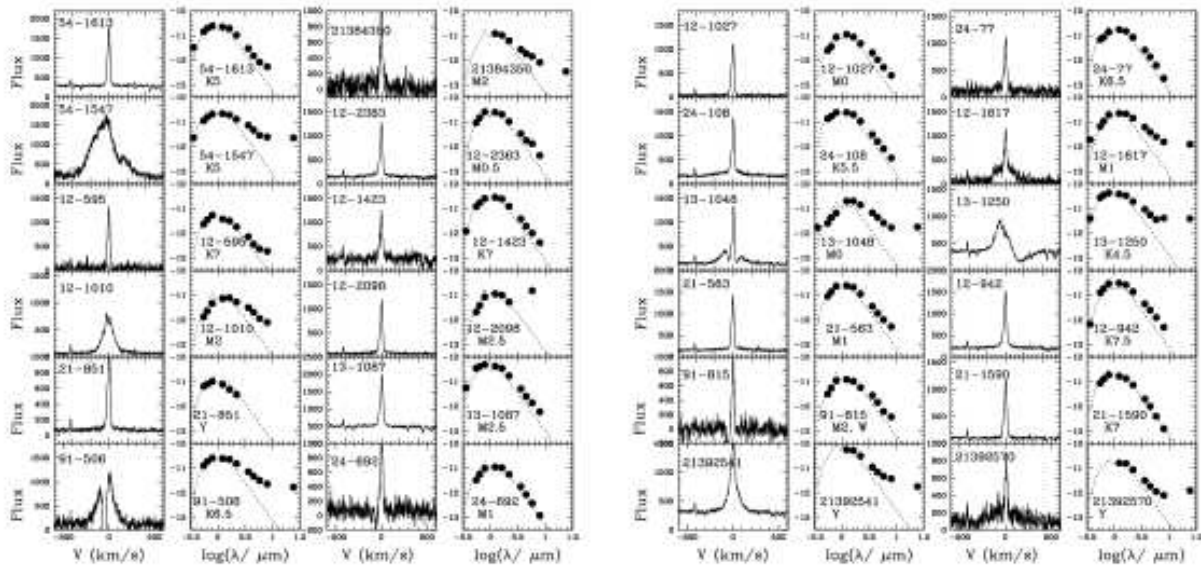


Fig. 5.—  $H\alpha$  profiles and SEDs of the observed members and potential members, showing the optical UVRI and JHK 2MASS fluxes (Paper I, II), IRAC (3.6, 4.5, 5.8, 8.0  $\mu\text{m}$ ; Paper III) and MIPS(24 $\mu\text{m}$ , 70  $\mu\text{m}$  for 13-277 only; Paper III) data. A photosphere (Kenyon & Hartmann 1995) for the given spectral type is displayed in each case to clarify the presence of an IR excess. The nebular emission was successfully subtracted from the broad  $H\alpha$  profiles with good S/N. Narrow  $H\alpha$  lines, as well as some low S/N broad profiles, are contaminated by the nebular emission. The units of the fluxes are counts (non-calibrated) for the  $H\alpha$  lines, and  $\log(\lambda F_\lambda)$  in  $\text{erg cm}^{-2} \text{s}^{-1}$  for the SEDs (continued).



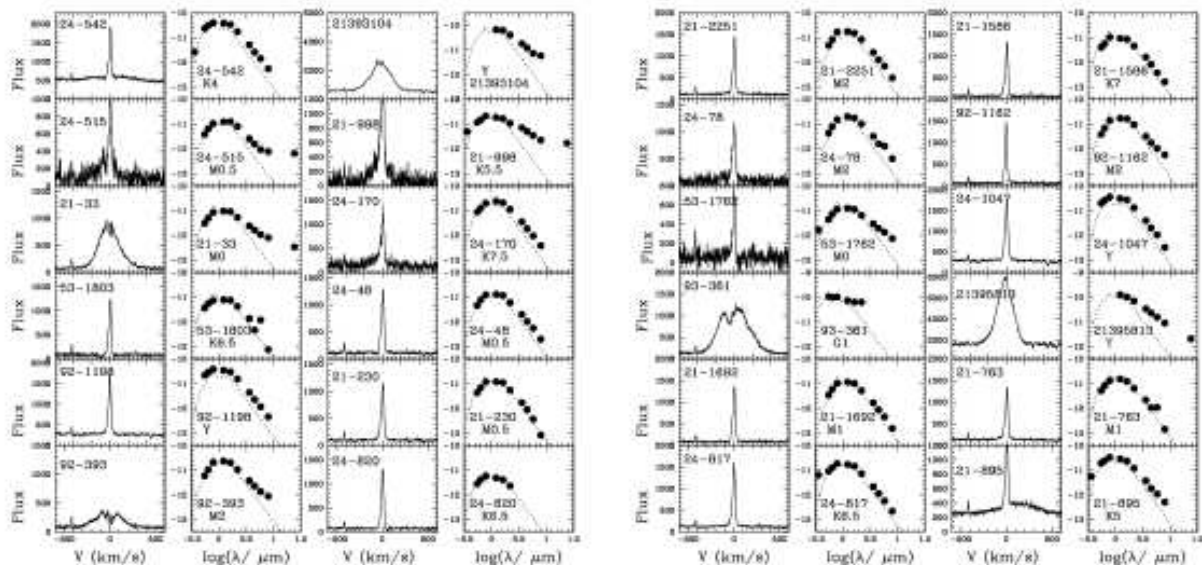


Fig. 6.—  $H\alpha$  profiles and SEDs of the observed members and potential members, showing the optical UVR-I and JHK 2MASS fluxes (Paper I, II), IRAC (3.6, 4.5, 5.8, 8.0  $\mu\text{m}$ ; Paper III) and MIPS(24 $\mu\text{m}$ ; Paper III) data. A photosphere (Kenyon & Hartmann 1995) for the given spectral type is displayed in each case to clarify the presence of an IR excess. The nebular emission was successfully subtracted from the broad  $H\alpha$  profiles with good S/N. Narrow  $H\alpha$  lines, as well as some low S/N broad profiles, are contaminated by the nebular emission. The units of the fluxes are counts (non-calibrated) for the  $H\alpha$  lines, and  $\log(\lambda F_\lambda)$  in  $\text{erg cm}^{-2} \text{s}^{-1}$  for the SEDs (continued).

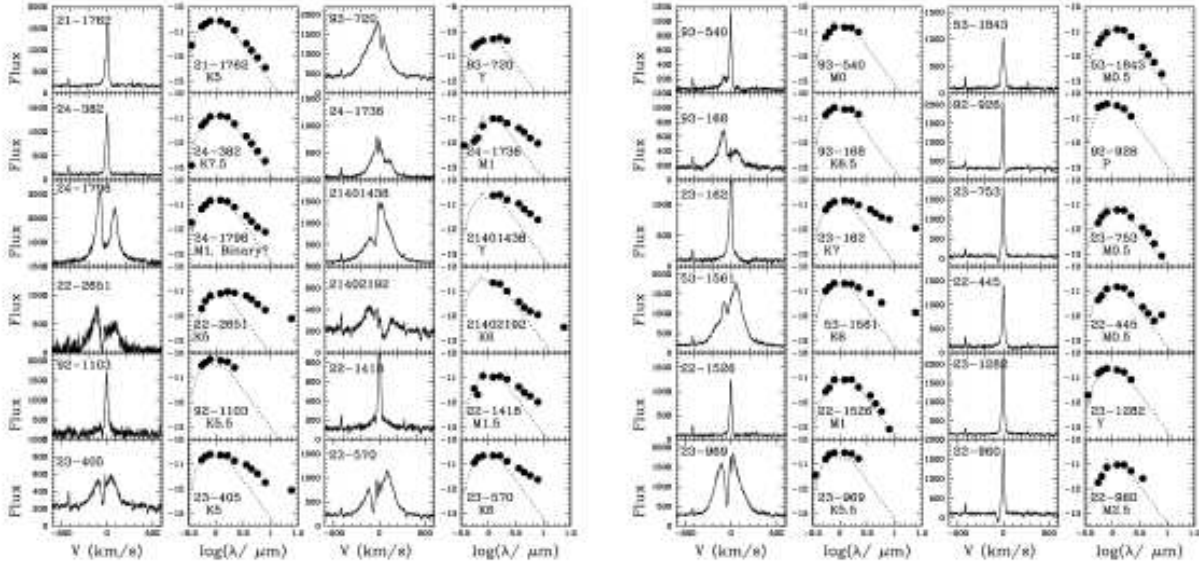


Fig. 7.—  $H\alpha$  profiles and SEDs of the observed members and potential members, showing the optical UVRI and JHK 2MASS fluxes (Paper I, II), IRAC (3.6, 4.5, 5.8, 8.0  $\mu\text{m}$ ; Paper III) and MIPS(24 $\mu\text{m}$ ; Paper III) data. A photosphere (Kenyon & Hartmann 1995) for the given spectral type is displayed in each case to clarify the presence of an IR excess. The nebular emission was successfully subtracted from the broad  $H\alpha$  profiles with good S/N. Narrow  $H\alpha$  lines, as well as some low S/N broad profiles, are contaminated by the nebular emission. The units of the fluxes are counts (non-calibrated) for the  $H\alpha$  lines, and  $\log(\lambda F_\lambda)$  in  $\text{erg cm}^{-2} \text{s}^{-1}$  for the SEDs (continued).

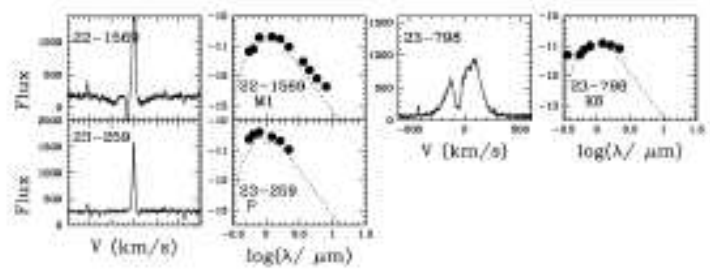


Fig. 8.—  $H\alpha$  profiles and SEDs of the observed members and potential members, showing the optical UVRI and JHK 2MASS fluxes (Paper I, II), IRAC (3.6, 4.5, 5.8, 8.0  $\mu\text{m}$ ; Paper III) and MIPS(24 $\mu\text{m}$ ; Paper III) data. A photosphere (Kenyon & Hartmann 1995) for the given spectral type is displayed in each case to clarify the presence of an IR excess. The nebular emission was successfully subtracted from the broad  $H\alpha$  profiles with good S/N. Narrow  $H\alpha$  lines, as well as some low S/N broad profiles, are contaminated by the nebular emission. The units of the fluxes are counts (non-calibrated) for the  $H\alpha$  lines, and  $\log(\lambda F_\lambda)$  in  $\text{erg cm}^{-2} \text{s}^{-1}$  for the SEDs (continued).

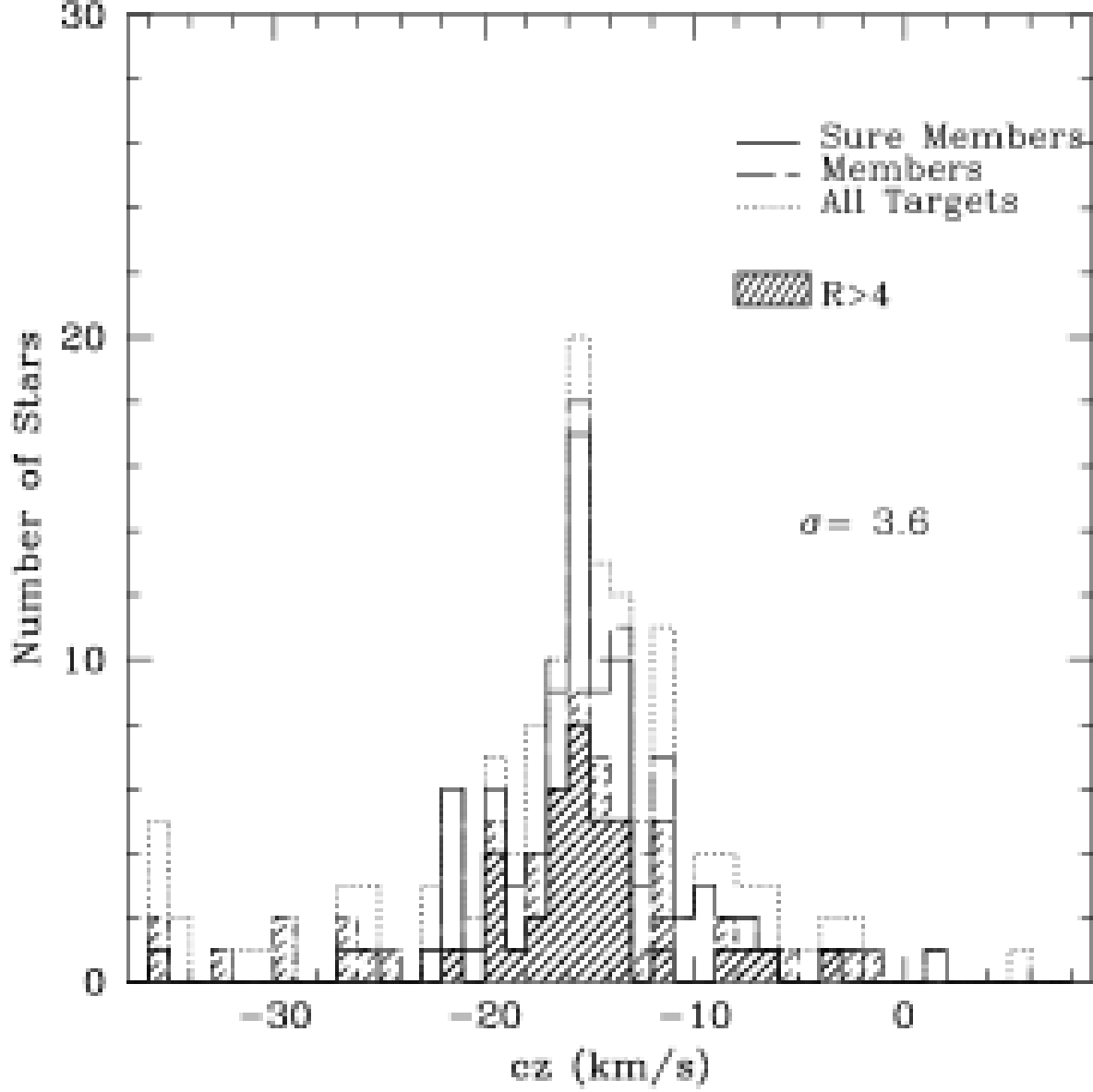


Fig. 9.— Radial velocity histogram for Tr 37. The radial velocities of sure members (confirmed by Li 6707Å in low-resolution spectra and/or broad H $\alpha$  lines, see text), sure and probable members (labeled “members”), and the rest of observed stars (“all targets”) are displayed in a histogram. Only velocities obtained through good cross-correlations are considered. Shaded areas represent the stars with  $R > 4$ . Using the sure members with  $R > 4$ , we obtain an average radial velocity for the cluster  $cz = -15.0 \pm 3.6$  km/s, where  $\sigma = 3.6$  km/s is the standard deviation.

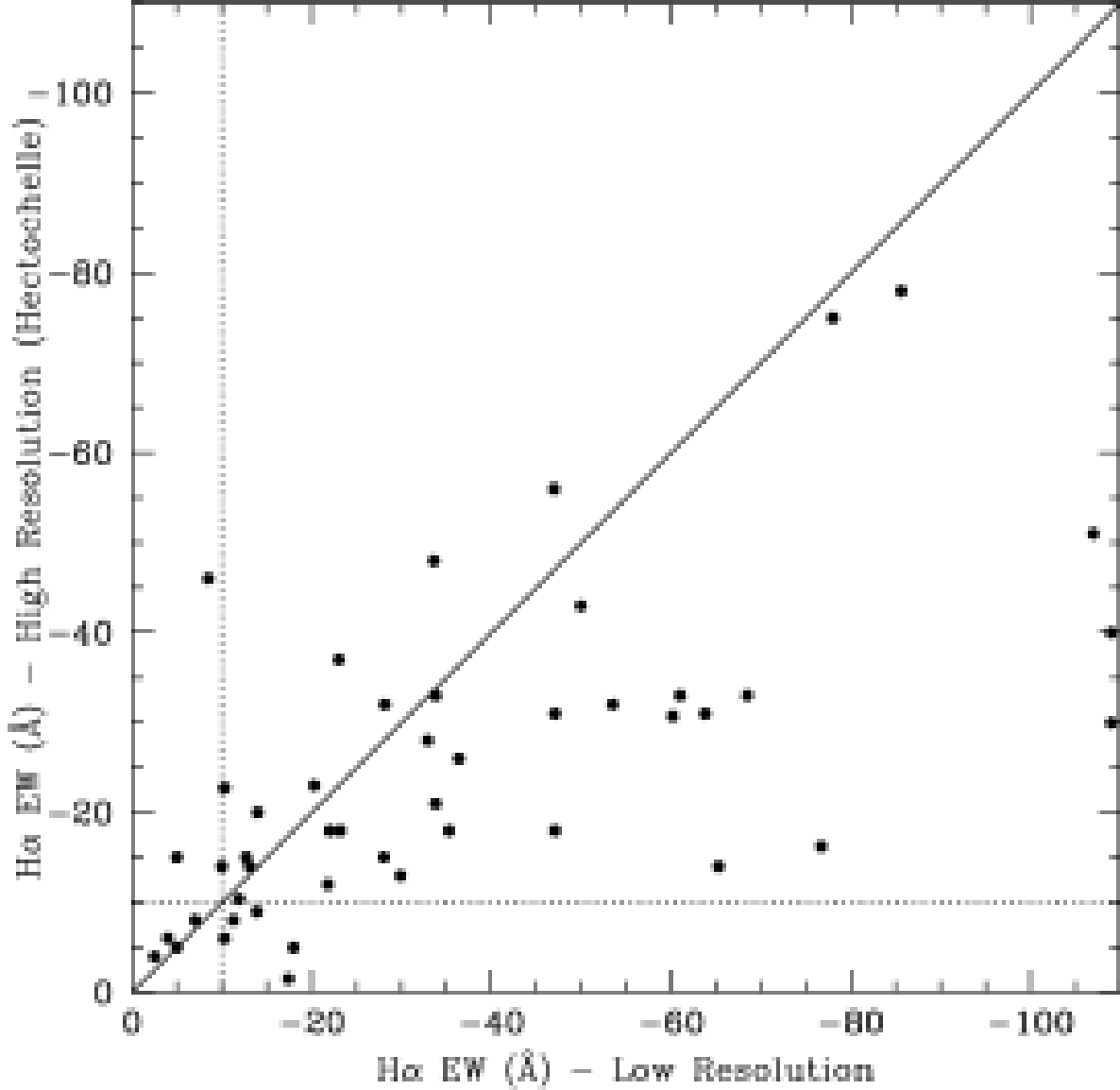


Fig. 10.— Comparison of the  $H\alpha$  EW (in  $\text{\AA}$ ) measured using low resolution (Hectospec and Hydra, see Paper I, II) and high resolution (Hectochelle) spectra. Note that we were able to measure the EW only for spectra with broad  $H\alpha$  lines. Therefore, all objects displayed are accreting stars or CTTS. The dotted lines indicate  $\text{EW} = -10\text{\AA}$  which is the classical limit for distinguishing CTTS and WTTS, although we find several broad-lined stars with smaller EW. The dispersion between the  $H\alpha$  values measured with low and high resolution is mostly due to the intrinsic variations of the stars (Sicilia-Aguilar et al. 2005). Some extreme values of  $H\alpha$  measured from low-resolution spectra are caused by poor S/N, which produces very low continuum in the region. Note that some variation can be introduced because of poor continuum estimates in cases of low S/N (see Paper I, Paper II for more details), resulting in large ( $\sim 60\text{--}100\text{\AA}$ ) EW that are not real.

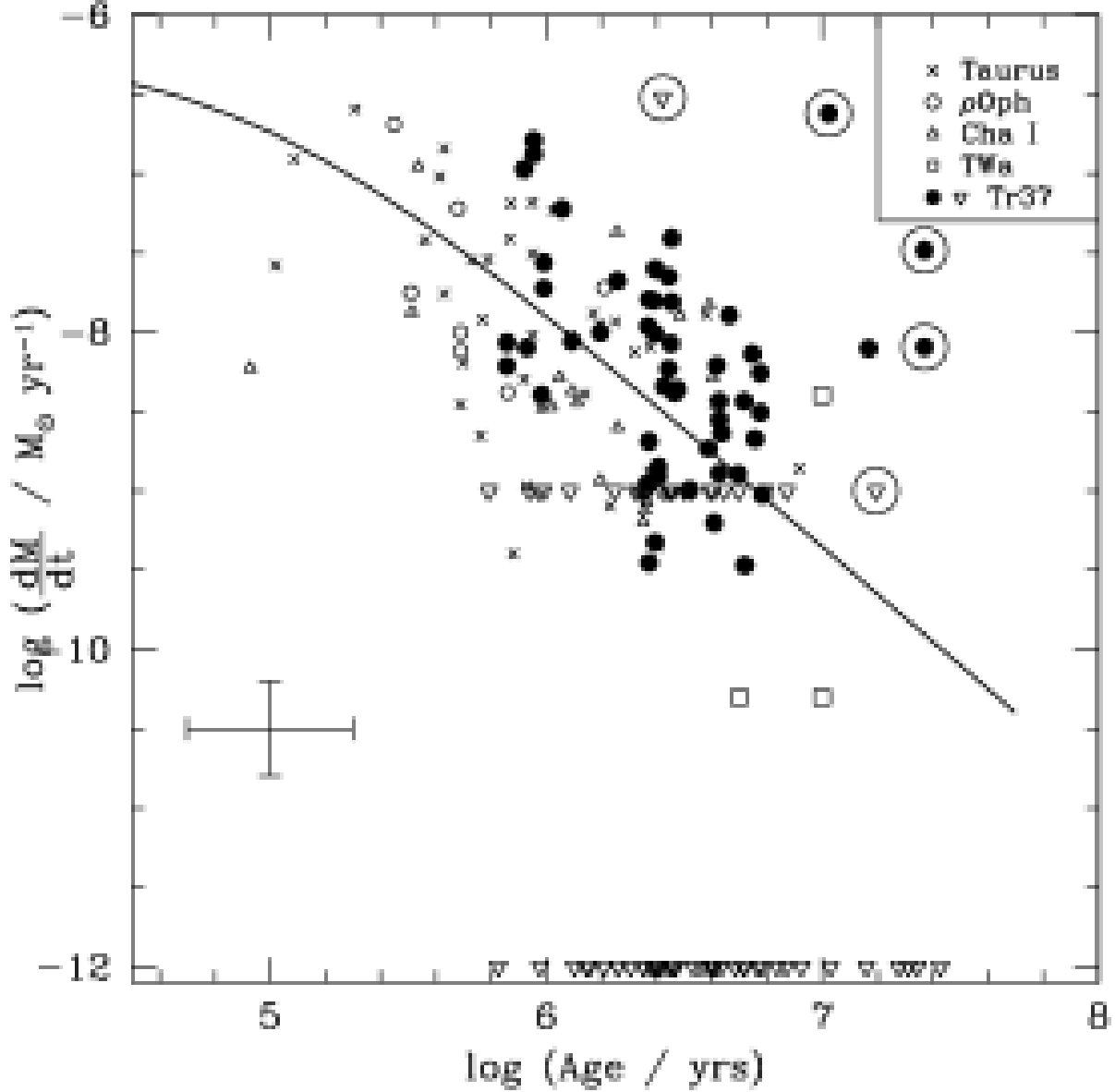


Fig. 11.— Accretion rate vs. age in Tr 37. Filled circles represent stars with accretion rates derived from U band (see Paper I, PaperII for a discussion about the accretion rate estimates). Open triangles are upper limits to the accretion based on the presence of broad  $H\alpha$  emission ( $10^{-9}M_{\odot}/\text{yr}$ ) in stars for which we did not find any U excess (U band observations were complete to approximately the U photospheric emission of a K6 star), and the lack of broad components in stars with no U excess ( $10^{-12}M_{\odot}/\text{yr}$ ). For comparison, we include data from other regions and the model for the evolution of a viscous disk (Hartmann et al. 1998; Muzerolle et al. 2000). The average accretion rate in Tr 37 (including the upper limits, but excluding the G-type stars, marked here with large open circles) is  $9 \times 10^{-9} M_{\odot}/\text{yr}$ . The typical error bar for  $\dot{M}$  derived from U band and for the age is displayed.

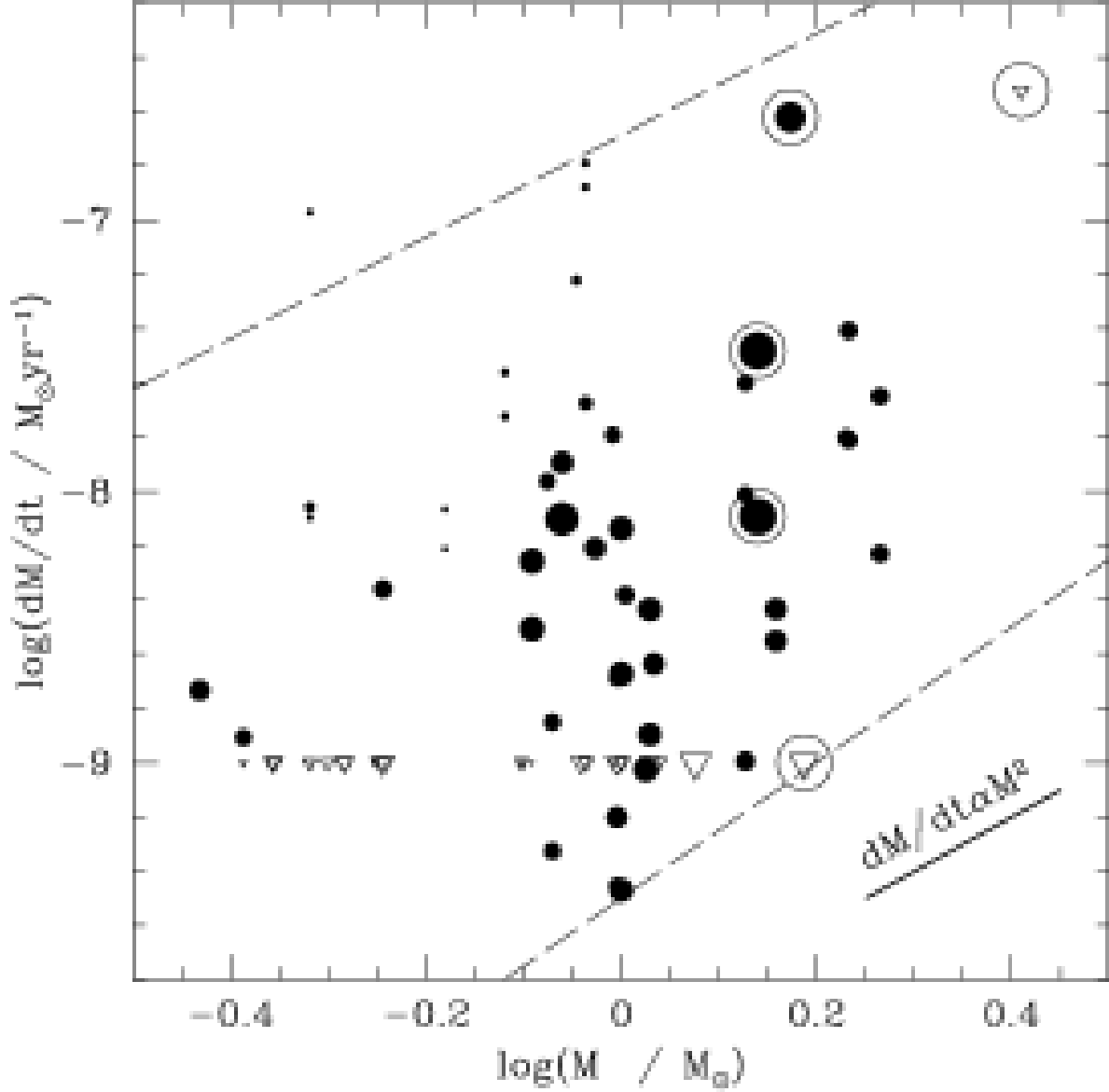


Fig. 12.— Accretion rate vs. mass in Tr 37. The size of the dots and open triangles (upper limits) is proportional to the age. Very small dots represent the globule population (aged  $\sim 1$  Myr). Ages for G-type stars tend to look larger ( $\sim 10$  Myr, G stars are marked by large open circles) but are highly uncertain. The data is consistent with the study of Calvet et al. (2004), whose data is comprised between the dashed lines, and with the  $\dot{M} \propto M^2$  trend observed by Natta et al. (2004), although our sample contains stars spanning a smaller parameter area in both accretion rate and mass. This trend appears independently of age in both the globule and the bulk (4 Myr old in average) population, even though accretion rates for the younger stars tend to be higher, as expected from the viscous disk evolutionary models (Hartmann et al. 1998).

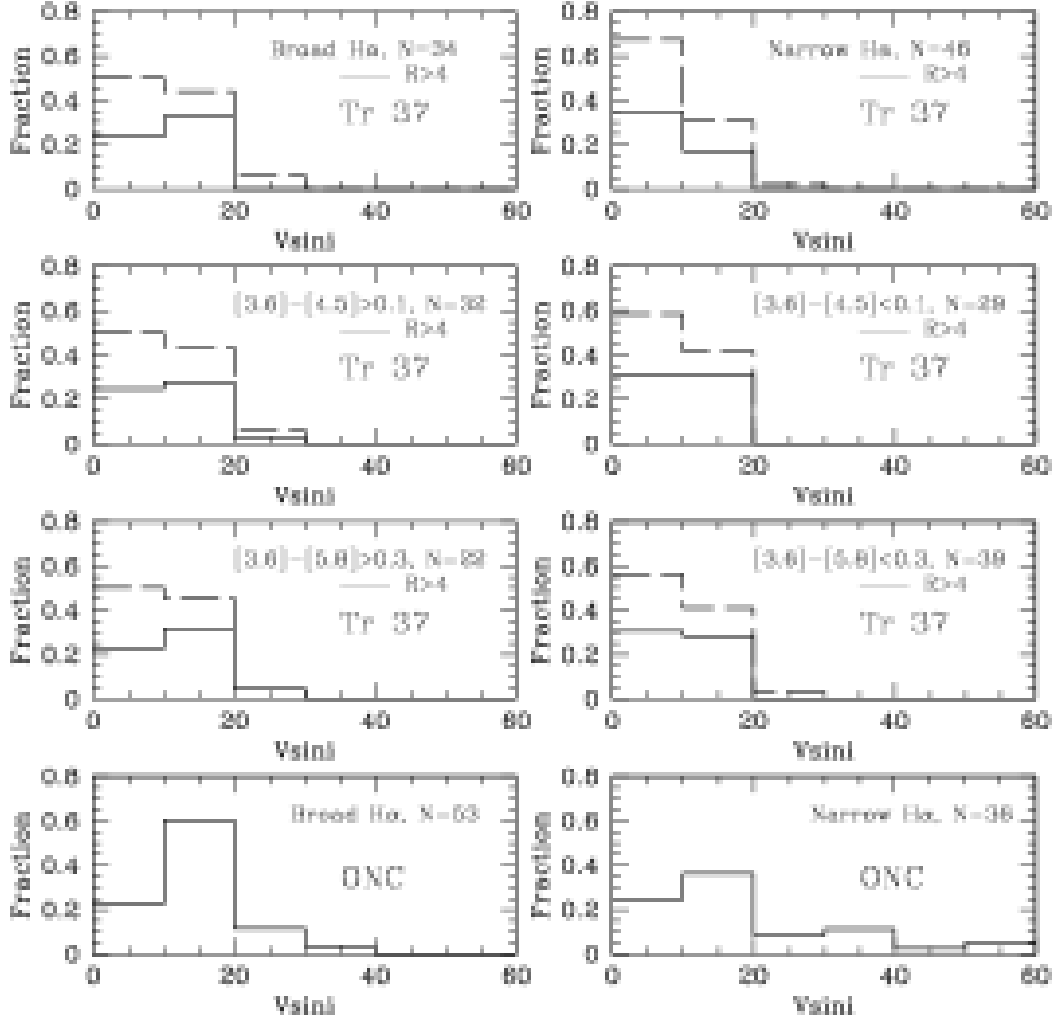


Fig. 13.— Rotational velocities of stars with disks versus stars without disks. The fraction of stars in each velocity bin ( $V_{\sin i}$  in km/s) is given for three different definitions of disk in Tr 37, displayed in the three upper rows of figures. Figures on the left correspond to accreting and/or disked stars (typically, CTTS), figures on the right correspond to non-accreting and/or diskless stars (typically, WTTS). In the two upper panels, we compare stars with broad and narrow  $H\alpha$ . The second row of panels defines the presence of a disk as an excess in the IR such that the Spitzer color  $[3.6]-[4.5]$  is larger/ smaller than 0.1. The third row distinguishes stars with  $[3.6]-[5.8]$  colors larger/smaller than 0.3 (see Paper III for an explanation of CTTS versus WTTS typical colors). The fourth row shows the histograms for stars with broad versus narrow  $H\alpha$  emission in the ONC (Sicilia-Aguilar et al. 2005). We do not find substantial difference in the rotation of CTTS vs. WTTS in Tr 37, and the differences with the stars in the ONC may result from the differences in the ages, cluster morphology, and also because of the effect of poorer S/N (see text).



Table 1. Spectral Information

ID1	2MASS ID	Sp.Type	EW(H $\alpha$ Å)	EW(Li 6707 Å)	H $\alpha$ Type	H $\alpha$ 10% V(km/s)	R	cz (km/s)	Vsini (km/s)	Comments
71-1309	21340974+5729550	—	—	—	w	—	2.0:	-22.7 $\pm$ 2.1:	8.4:	PN(r)*
74-48	21344730+5731148	—	—	—	w	—	4.2	-8.5 $\pm$ 1.1	7.6	P(r)*
73-758	21350835+5736028	K6.5	(-9)	0.4	w:	—	2.6	1.7 $\pm$ 1.6	7.7	Y(e),N(r),TOn:
72-1427	21351627+5728222	M1	-16(-77)	—	c	330	1.5:	122.0 $\pm$ 1.7:	5.6:	Y(e),N(r)
81-541	21351745+5748223	K5.5	-31(-60)	0.4	c	380	—	—	—	Y(e)
64-156	21351804+5709441	—	—	—	w	—	3.7	-8.1 $\pm$ 1.2	7.4	P(r)*
73-472	21351861+5734092	K5	-23(-10)	0.7	c	300	3.4	-17.1 $\pm$ 1.7	9.6	Y(e),Y(r)
73-674	21352076+5735288	—	—	—	w	—	9.3	-24.5 $\pm$ 0.5	7.2	PN(r)*
73-1059	21352386+5738145	—	—	—	w	—	5.3	-12.8 $\pm$ 1	8.6	Y(r)*
73-311	21352451+5733011	M1.5	(-29)	—	c	—	—	—	—	Y(e)
73-71	21353021+5731164	K6	-10(-12)	0.4	c	380	3.7	-11.5 $\pm$ 3.6	24.4	Y(e),Y(r)
72-875	21354975+5724041	M0.5	(-21)	0.1:	w(c)	—	1.6	17.3 $\pm$ 2	7	Y(e),N(r),SB1:
61-608	21355070+5703570	—	—	—	w	—	4.4	-15.6 $\pm$ 1.2	8.2	Y(r)*
64-376	21355082+5712071	—	—	—	w	—	3	-22.2 $\pm$ 1.5	7.8	PN(r)*
73-194	21355223+5732145	K6.5	(-4)	—	w	—	3.4	-14.4 $\pm$ 1.2	7.3	P(e),Y(r),TOn
61-893	21360090+5707129	—	—	—	w	—	2.3:	-9.8 $\pm$ 2.2:	9.9:	P(r)*
73-537	21360723+5734324	G1.5	(-5)	0.3	w(c)	—	3.1	-20.5 $\pm$ 2.2	11.7	Y(e),P(r)
84-23	21361281+5753004	—	—	—	w	—	3.8	-18.3 $\pm$ 1.5	9.6	Y(r)*
—	21362368+5732452	—	—	—	w	—	1.6:	-11.7 $\pm$ 2.3:	7.7:	Y(r)*
—	21362507+5727502	M0	-78:(-86)	—	c	—	2.4	-68.9 $\pm$ 1.7	7.6	Y(e),N(r),SB1
61-413	21362615+5701293	—	—	—	w	—	3.2	-25.6 $\pm$ 0.9	5.2	PN(r)*
14-306	21362676+5732374	K6.5	(-8)	—	w	—	—	—	—	P(e)
—	21364596+5729339	ClassI	-47	—	w:(c)	—	1.4:	-11.8 $\pm$ 1.8:	5.7:	Y(e),Y(r)
—	21364762+5729540	K6	(-76)	0.5	w(c)	—	—	—	—	P(e)
14-141	21364941+5731220	K6	-15(-5)	0.6	c	570	2.3:	-9.2 $\pm$ 3.6:	27.0:	Y(e),P(r)
14-1229	21365579+5736533	K6	(-5)	0.4	w	—	—	—	—	Y(e)
11-2146	21365767+5727331	K6	-28(-33)	0.5	c	470	7.6	-15.4 $\pm$ 1.1	12.6	Y(e),Y(r)
11-1209	21365850+5723257	K6	-6(-4)	0.7	c(w)	350	10	-8.4 $\pm$ 0.8	12.2	Y(e),P(r)

Table 1—Continued

ID1	2MASS ID	Sp.Type	EW(H $\alpha$ Å)	EW(Li 6707 Å)	H $\alpha$ Type	H $\alpha$ 10% V(km/s)	R	cz (km/s)	Vsini (km/s)	Comments
—	21365947+5731349	M0	-30(-109)	—	c	510	—	—	—	Y(e)
11-1659	21370088+5725224	K5	(-2)	0.5	w	—	7.7	-14.6 $\pm$ 0.8	9.1	Y(e),Y(r)
11-1499	21370140+5724458	M1.5	(-7)	0.3:	w	—	—	—	—	Y(e)
11-2322	21370191+5728222	M1	-18(-23)	0.4	c	420	2.7:	-9.9 $\pm$ 2.0:	9.5:	Y(e),P(r)
11-1871	21370254+5726144	M2	(-13)	1	w(c)	—	—	—	—	Y(e)
14-222	21370607+5732015	K7	(-5)	0.6	w	—	—	—	—	Y(e),TOn:
14-287	21370649+5732316	M0	-18(-35)	0.5	c	470	2.9	-15.7 $\pm$ 2.1	11	Y(e),Y(r)
11-2037	21370703+5727007	K4.5	-43(-50)	0.5	c	420	9.8	-19.9 $\pm$ 0.6	8.6	Y(e),P(r)
11-1067	21370843+5722484	M0.5	(-7)	—	w	—	—	—	—	Y(e)
14-11	21371031+5730189	M1.5	(-5)	0.3	w	—	2	-15.0 $\pm$ 3.7	15.1	Y(e),Y(r),TOn
14-125	21371054+5731124	K5	-14(-13)	0.6	c	320	2.8	-16.7 $\pm$ 1.1	5.6	Y(e),Y(r)
11-1513	21371183+5724486	K7.5	(-5)	0.5	w	—	—	—	—	Y(e)
11-2131	21371215+5727262	K6.5	(-10)	0.5	c	—	—	—	—	Y(e)
11-2487	21371498+5729123	K7	(-4)	0.4	w	—	—	—	—	Y(e)
11-2031	21371591+5726591	K2	-5(-5)	0.4	c	440	6.8	-17.2 $\pm$ 1.2	12.6	Y(e),Y(r)
14-103	21371976+5731043	K7	(-2)	0.3	w	—	—	—	—	Y(e)
14-197	21372368+5731538	K5.5	(-2)	0.5	w	—	2.1:	-25.0 $\pm$ 3.9:	20.4:	Y(e),PN(r),SB1:
—	21372410+5724115	—	-60	—	c	430	—	—	—	Y(e)*
14-160	21372732+5731295	K5	(-22)	0.6	c:(c)	—	4.3	-16.7 $\pm$ 2.9	22.5	Y(e),Y(r)
11-581	21372828+5720326	G	(-9)	—	w	—	6.7	-68.2 $\pm$ 0.7	6.7	P(e),N(r),rej
14-1017	21372894+5736042	M0	(-55)	0.5	c	—	—	—	—	Y(e)
14-335	21372915+5732534	K6.5	(-20)	0.6	w:(c)	—	—	—	—	Y(e)
11-1864	21373420+5726154	G-K	(-5)	0.3	w(c)	—	3.1	-42.8 $\pm$ 1.7	9.5	Y(e),N(r),SB1
83-343	21373696+5755149	M0.5	(-3)	0.5	c:(w)	—	3.5	-21.3 $\pm$ 1.5	8.8	Y(e),P(r)
14-183	21373849+5731408	K7.0(K5)	-14(-65)	1.2:	c	490	2.2	-22.4 $\pm$ 3	12.8	Y(e),PN(r),SB1:
14-995	21373987+5736029	—	—	—	w	—	1.9:	-7.5 $\pm$ 1.6:	6.0:	PN(r)*
14-2148	21374184+5740400	M1.5	(-2)	0.4	w	—	1.8:	-21.3 $\pm$ 1.3:	4.8:	Y(e),P(r),TOn:
—	21374275+5733250	F9	-32(-54)	0.1:	c	380	—	—	—	Y(e)

Table 1—Continued

ID1	2MASS ID	Sp.Type	EW(H $\alpha$ Å)	EW(Li 6707 Å)	H $\alpha$ Type	H $\alpha$ 10% V(km/s)	R	cz (km/s)	Vsini (km/s)	Comments
11-1384	21374486+5724135	K6.5	(-5)	0.6	w	—	—	—	—	Y(e)
11-383	21374514+5719423	K5	-37(-23)	0.3	c	270	—	—	—	Y(e)
—	21374893+5723209	—	-42	—	c	540	—	—	—	Y(e)*
13-924	21375018+5733404	K5	(-4)	0.6	w	—	3.4	-20.3 $\pm$ 1.5	8.8	Y(e),P(r)
12-1984	21375022+5725487	K6	(-5)	0.7	w	—	—	—	—	Y(e)
12-2519	21375107+5727502	K5.5	(-8)	0.5	w(c)	—	2.6	-18.5 $\pm$ 2.2	10.5	Y(e),Y(r)
12-1968	21375487+5726424	K6	-8(-11)	0.4:	c	390	6.9	-16.9 $\pm$ 1	10.9	Y(e),Y(r),SB2:
12-1422	21375756+5724197	M0	(-17)	0.7	w(c)	—	—	—	—	Y(e)
12-1091	21375762+5722476	G2.5	-2(-17)	0.5	c	—	6.1	-15.8 $\pm$ 0.9	8.8	Y(e),Y(r)
13-269	21375812+5731199	K6.5	(-7)	0.4	w	—	—	—	—	Y(e)
12-583	21375827+5720354	M0	(-7)	—	w	—	—	—	—	Y(e)
12-94	21375841+5718046	K4	(-4)	—	w	—	7.7	-117.9 $\pm$ 0.6	6.4	P(e),N(r),rej
12-94	21375841+5718046	K4	(-4)	—	w	—	—	—	—	P(e)
13-1143	21375852+5735479	—	—	—	w	—	5.7	-11.2 $\pm$ 0.8	7.2	P(r)*
13-1238	21375926+5736162	M1	-31(-64)	0.7	c	550	—	—	—	Y(e)
12-2373	21380058+5728253	M1	(-6)	0.4	w	—	2.6	-16.7 $\pm$ 2.1	10	Y(e), Y(r)
82-272	21380350+5741349	G9	-15(-13)	0.4	c	—	2.6	-15.6 $\pm$ 3.8	18.1	Y(e)Y(r),SB2
12-1081	21380593+5722438	M0.5	(-4)	0.7	w	—	—	—	—	Y(e)
13-1161	21380772+5735532	M0	(-1)	0.5	w	—	2.2:	-21.8 $\pm$ 3.0:	12.8:	Y(e),P(r)
12-1613	21380848+5725118	M1	(-13)	—	w(c:)	—	—	—	—	P(e)
13-1426	21380856+5737076	M0	-40(-109)	—	c	460	—	—	—	Y(e)
—	21380924+5720198	—	-17	—	c	490	1.6:	-22.0 $\pm$ 2.4:	8.2:	Y(e),P(r)*
13-669	21380928+5733262	K1	-18(-22)	0.6	c	500	9.3	-21.3 $\pm$ 1	14.2	Y(e),P(r)
—	21380979+5729428	—	—	—	w:	—	2.9	-17.3 $\pm$ 1.7	9	Y(r)*
13-838	21381120+5734181	—	—	—	w	—	2.1	-6.3 $\pm$ 1.6	6.6	PN(r)*
13-350	21381384+5731414	M1	(-9)	—	w	—	2.9	-12.6 $\pm$ 1.2	6.4	P(e),Y(r), conf,TO
13-350	21381384+5731414	M1	(-9)	—	w	—	1.9:	-16.9 $\pm$ 1.8:	7.1:	P(e),Y(r), conf,TO
12-1017	21381509+5721554	K5.5	(-4)	0.6	w	—	9.8	-15.1 $\pm$ 0.6	8.8	Y(e),Y(r)

Table 1—Continued

ID1	2MASS ID	Sp.Type	EW(H $\alpha$ Å)	EW(Li 6707 Å)	H $\alpha$ Type	H $\alpha$ 10% V(km/s)	R	cz (km/s)	Vsini (km/s)	Comments
54-1781	21381612+5719357	M1	(-13)	0.3:	c:(c)	—	2.1	-15.6 $\pm$ 1.7	7.1	Y(e),Y(r)
54-1781	21381612+5719357	M1	(-13)	0.3:	c:(c)	—	1.7:	-13.4 $\pm$ 2.2:	8.1:	Y(e),Y(r)
13-1877	21381703+5739265	K7	-33(-68)	0.4	c	430	—	—	—	Y(e)
13-277	21381731+5731220	G1	-14(-10)	—	c	660	4.5	-7.5 $\pm$ 6.7	51.6	Y(e),PN(r),SB1:
13-2236	21381749+5741019	K6.5	(-1)	0.6	w	—	5.4	-13.8 $\pm$ 1.6	15.2	Y(e),Y(r)
12-1009	21381750+5722308	K5.5	(-4)	0.6	w	—	3.7	-18.4 $\pm$ 2	12.6	Y(e),Y(r)
94-1119	21381862+5803283	—	—	—	w	—	11.2	-19.0 $\pm$ 0.5	7.3	P(r)*
13-819	21382596+5734093	K5.5	-6(-10)	0.5	c	—	—	—	—	Y(e),TOa
94-1050	21382668+5802377	—	—	—	w	—	2	-13.1 $\pm$ 1.9	7.8	Y(r)*
12-1955	21382692+5726385	K6.5	(-2)	0.4	w	—	7.5	-19.1 $\pm$ 0.8	9	Y(e),P(r)
13-236	21382742+5731081	K2	-56(-47)	—	c	500	9.3	-18.2 $\pm$ 0.7	9	Y(e),Y(r)
12-2113	21382743+5727207	K6	-15(-28)	0.4	c	430	3.7	-26.1 $\pm$ 1.8	11.7	Y(e),N(r),SB1
13-157	21382804+5730464	K5.5	-20(-14)	0.5	c	560	3.8	-15.6 $\pm$ 1.3	8.7	Y(e),Y(r)
13-232	21382834+5731072	M0	(-3)	0.3:	w	—	—	—	—	Y(e)
—	21383216+5726359	M0	(-129)	0.3:	c	—	—	—	—	P(e)
13-52	21383255+5730161	K7	(-1)	0.7	w	—	3.2	-19.1 $\pm$ 1.5	8.1	Y(e),P(r),TOOn
12-1825	21383382+5726053	—	—	—	w	—	2.4	-15.8 $\pm$ 2	8.8	Y(r)*
91-155	21383470+5741274	M2.5	(-8)	0.4	w	—	1.5	-9.3 $\pm$ 1.9	5.9	Y(e),P(r)
13-566	21383481+5732500	K5.5	(-5)	0.4	w	—	—	—	—	Y(e),TOOn
13-1891	21384001+5739303	M0	(-11)	—	c	—	3.3	-13.8 $\pm$ 1.8	10.1	P(e),Y(r),conf
13-1709	21384038+5738374	K5.5	(-3)	0.4	w	—	3.3	-15.6 $\pm$ 1.8	10.4	Y(e),Y(r)
54-1613	21384332+5718359	K5	(-1)	0.5	w	—	12.3	-16.5 $\pm$ 0.5	9.5	Y(e),Y(r),TOOn:
—	21384350+5727270	M2	(-23)	0.4	w(c)	—	—	—	—	Y(e),TOOn
54-1547	21384446+5718091	K5.5	-33(-34)	0.4	c	540	1.8	-15.7 $\pm$ 4.9	20	Y(e),Y(r)
12-2363	21384544+5728230	M0.5	(-3)	0.6	w	—	2.7	-7.4 $\pm$ 4.7	27.1	Y(e),PN(r),SB1:
12-595	21384622+5720380	K7	(-17)	1.6	w(c)	—	—	—	—	Y(e),TOOn:
12-1423	21384707+5724207	K7	(-2)	0.5	w	—	4	-15.6 $\pm$ 1.1	7.5	Y(e),Y(r)
12-1010	21385029+5722283	M2	-23(-20)	0.2:	c	270	2.5	-16.5 $\pm$ 1.8	8.2	Y(e),Y(r)

Table 1—Continued

ID1	2MASS ID	Sp.Type	EW(H $\alpha$ Å)	EW(Li 6707 Å)	H $\alpha$ Type	H $\alpha$ 10% V(km/s)	R	cz (km/s)	Vsini (km/s)	Comments
12-2098	21385253+5727184	M2.5	(-7)	0.7	w	—	—	—	—	Y(e)
21-851	21385504+5720423	—	—	—	w	—	1.5	-17.5 $\pm$ 1.8	6	Y(r)*
13-1087	21385542+5735299	K4	(-2)	0.6	w	—	12.7	-15.0 $\pm$ 0.6	11.2	Y(e),Y(r)
91-506	21385807+5743343	K6.5	-31(-47)	0.6	c	450	3.1	-15.8 $\pm$ 1.5	8.4	Y(e),Y(r)
24-692	21390054+5734280	M1	(-2)	0.5	w	—	2.1	-35.0 $\pm$ 1.5	6	Y(e),N(r),SB1
12-1027	21390319+5722318	M0	(-11)	0.8	w(c)	—	—	—	—	Y(e)
24-77	21390346+5730527	K6.5	(-3)	0.5	w	—	—	—	—	Y(e)
24-108	21390390+5731037	K5.5	(-3)	0.4	w	—	—	—	—	Y(e)
12-1617	21390468+5725128	M1	-13(-30)	0.6	c	—	1.7:	-13.4 $\pm$ 1.7:	6.1:	Y(e),Y(r)
12-1650	21390471+5725215	—	—	—	w	—	6.7	-25.2 $\pm$ 0.8	7.8	PN(r)*
13-1048	21391088+5735181	M0	-8(-7)	0.4	c(w)	430	6.6	-16.1 $\pm$ 1.1	10.9	Y(e),Y(r)
13-1250	21391213+5736164	K4.5	-4(-2)	0.4	c(w)	540	9.7	-15.7 $\pm$ 0.6	8.3	Y(e),Y(r),TOa
21-563	21391288+5721088	M1	(-2)	0.3	w(c)	—	—	—	—	Y(e)
12-942	21391424+5722129	K7.5	(-4)	0.7	w	—	4.1	-4.0 $\pm$ 2.7	19.3	Y(e),N(r),SB1
91-815	21391465+5745177	M2	(-4)	0.2:	w	—	2	-17.1 $\pm$ 1.6	6.5	Y(e),Y(r)
21-1590	21391554+5726440	K7	(-4)	0.6	w	—	4.3	-17.3 $\pm$ 1.5	10.6	Y(e),Y(r)
21-1189	21391583+5724350	—	—	—	w	—	2.1:	-7.0 $\pm$ 2.0:	8.7:	PN(r)*
—	21392541+5733202	—	—	—	c	200	8.1	-14.4 $\pm$ 0.7	8.8	Y(r),TOa
—	21392570+5729455	—	—	—	w:	—	2.2:	-15.0 $\pm$ 1.7:	7.5:	Y(r)*,TOa
24-542	21392957+5733417	K4	(-4)	1.3	w	—	—	—	—	Y(e)
—	21393104+5747140	—	-16	—	c	450	15.5	-15.8 $\pm$ 0.4	8.8	Y(e),Y(r)*
24-515	21393407+5733316	M0.5	(-11)	—	c	—	1.9:	-19.4 $\pm$ 2.0:	7.6:	Y(e),P(r),TOa
21-998	21393480+5723277	K5.5	(-16)	0.3:	c	—	1.6	-78.8 $\pm$ 2.1	7.3	Y(e),N(r),SB1:
21-33	21393561+5718220	M0	-51(-107)	—	c	450	1.8:	-13.2 $\pm$ 2.4:	8.9:	Y(e),Y(r)
24-170	21393612+5731289	K7.5	(-4)	0.4	w	—	1.5:	-14.4 $\pm$ 2.2:	7.0:	Y(e),Y(r)
53-1803	21393803+5719332	K6.5	(-1)	0.4	w	—	3.5	-107.9 $\pm$ 1.2	7.2	Y(e),N(r),SB1
24-48	21393805+5730439	M0.5	(-1)	0.5	w	—	6.2	-15.1 $\pm$ 0.8	8.1	Y(e),Y(r)
92-1198	21394009+5746561	—	—	—	w	—	7.7	-17.0 $\pm$ 1.2	14.1	Y(r)*

Table 1—Continued

ID1	2MASS ID	Sp.Type	EW(H $\alpha$ Å)	EW(Li 6707 Å)	H $\alpha$ Type	H $\alpha$ 10% V(km/s)	R	cz (km/s)	Vsini (km/s)	Comments
21-230	21394169+5719274	M0.5	(-3)	0.5	w	—	4.3	-14.3 $\pm$ 1.6	11.3	Y(e),Y(r)
92-393	21394408+5742159	M2	-21(-34)	—	c	520	2.4	-15.8 $\pm$ 2.9	14.2	Y(e),Y(r),TOa
24-820	21394746+5735059	K6.5	(-2)	—	w	—	4.1	-11.0 $\pm$ 1	6.9	P(e),P(r),conf
21-2251	21394754+5725210	M2	(-4)	0.4:	w	—	1.8:	-2.6 $\pm$ 4.4:	16.7:	Y(e),N(r),SB1:
21-1586	21394793+5726427	K7	(-16)	0.9	w(c)	—	2.8	-10.7 $\pm$ 1.9	9.4	Y(e),P(r)
24-78	21394936+5730546	M2	(-6)	0.3	w	—	2.1:	-21.6 $\pm$ 2.9:	12.0:	Y(e),P(r)
92-1162	21394974+5746468	M2	(-7)	0.5	w	—	2.7:	-12.4 $\pm$ 1.6:	8.0:	Y(e),Y(r)
53-1762	21395029+5719177	M0	(-2)	0.4	w	—	1.9:	-73.1 $\pm$ 2.1:	8.0:	Y(e),N(r),SB1:
24-1047	21395088+5736168	—	—	—	w	—	7.5	-14.9 $\pm$ 1.3	14.7	Y(r)*
93-361	21395237+5756186	G1	-75(-78)	0.4	c	—	—	—	—	Y(e)
—	21395813+5728335	—	-15	—	c	370	11.1	-19.0 $\pm$ 0.7	11.8	Y(e),P(r)*
21-1692	21400128+5727184	M1	(-5)	0.5	w	—	4.4	-16.5 $\pm$ 1.2	8.9	Y(e),Y(r)
21-763	21400259+5722090	M0	(-3)	0.4	w	—	2.5	-14.7 $\pm$ 5.5	28.3	Y(e),Y(r)
24-817	21400273+5735050	K6.5	(-4)	0.6	w	—	4.2	-16.4 $\pm$ 2.2	15	Y(e),Y(r)
21-895	21400321+5722505	K5	(-1)	0.5	w	—	—	—	—	Y(e)
21-1762	21400924+5727393	K5	(-3)	0.5	w	—	6.2	-11.8 $\pm$ 1.3	12.3	Y(e),Y(r)
93-720	21400999+5800036	—	-16	—	c	470	10.3	-6.2 $\pm$ 0.8	12.5	Y(e),PN(r)*
24-382	21401023+5732511	K7.5	(-5)	0.4	w	—	6.2	-13.1 $\pm$ 0.9	8.4	Y(e),Y(r)
24-1736	21401134+5739518	M1	-33(-61)	—	c	380	1.9:	-11.4 $\pm$ 1.8:	6.9:	Y(e),Y(r)
24-1796	21401182+5740121	K7	-73(-124)	0.3	c	410	1.4:	-12.9 $\pm$ 4.1:	13.2:	Y(e),Y(r),SB2:
—	21401438+5740507	—	-46	—	c	470	2.6	-12.2 $\pm$ 1.8	8.7	Y(e),Y(r)*
22-2651	21402130+5726579	M1.5	-48(-34)	—	c	470	—	—	—	Y(e)
—	21402192+5730054	K6	-4(-8)	0.5	c(w)	510	9.3	-16.0 $\pm$ 0.8	10.6	Y(e),Y(r),TOa
92-1103	21402274+5746240	K5.5	(-7)	0.9	c:	—	3.1	-13.6 $\pm$ 1.6	9	Y(e),Y(r)
22-1418	21402287+5727329	M1.5	(-2)	0.5	c(w)	—	4.2	-13.9 $\pm$ 1.6	10.7	Y(e),Y(r)
92-582	21402592+5743271	—	—	—	w	—	4.6	-5.1 $\pm$ 1.1	8.6	PN(r)
23-405	21403134+5733417	K5	-9(-14)	0.4	c	410	6.9	-19.3 $\pm$ 1.2	12.8	Y(e),P(r)
23-570	21403574+5734550	K6	-18(-47)	0.4	c	520	9.5	-14.5 $\pm$ 0.6	8.2	Y(e),Y(r)

Table 1—Continued

ID1	2MASS ID	Sp.Type	EW(H $\alpha$ Å)	EW(Li 6707 Å)	H $\alpha$ Type	H $\alpha$ 10% V(km/s)	R	cz (km/s)	Vsini (km/s)	Comments
93-540	21403586+5758130	M0	-5 (-18)	0.3	c	290	2.9	-13.2 $\pm$ 1.5	7.6	Y(e),Y(r)
53-1843	21403592+5719398	M0.5	(-4)	0.6	w	—	3.1	-14.9 $\pm$ 2.1	11.4	Y(e),Y(r)
93-168	21404061+5754064	K6.5	-12(-22)	0.5	c	350	6.9	-13.5 $\pm$ 0.8	8.3	Y(e),Y(r)
92-926	21404150+5745219	—	—	—	w	—	12	-11.0 $\pm$ 0.4	6.9	P(r)*
23-162	21404450+5731314	K7	(-6)	0.4	c:(w)	—	5.6	-14.9 $\pm$ 0.8	7.4	Y(e),Y(r)
23-753	21405391+5736199	M0.5-M0	(-2)	0.5	w	—	2.8	-12.0 $\pm$ 1.7	8.3	Y(e),Y(r)
53-1561	21405592+5717591	K6	-32(-28)	0.1:	c	440	3.3	-11.0 $\pm$ 1.5	8.1	Y(e),P(r)
22-445	21405869+5721095	M0.5	(-4)	0.4	w	—	2.4	-9.0 $\pm$ 3.6	19.9	Y(e),P(r)
22-1526	21410212+5728220	M1	(-1)	0.5:	w	—	3.2	-15.8 $\pm$ 1.8	9.9	Y(e),Y(r)
23-1282	21410550+5741032	—	—	—	w	—	7	-17.0 $\pm$ 0.8	8.8	Y(r)*
23-969	21411497+5738149	K5.5	-26(-36)	0.5	c	460	8.8	-14.0 $\pm$ 0.8	10.9	Y(e),Y(r)
22-960	21411523+5724256	M2.5	(-3)	0.4:	w	—	—	—	—	P(e)
22-1569	21411837+5728433	M1	(-3)	0.6	w	—	6.3	-14.9 $\pm$ 0.8	7.5	Y(e),Y(r)
23-798	21412864+5736432	K6	-70(-150)	0.5	c	470	1.8:	-11.6 $\pm$ 1.6:	6.1:	Y(e),Y(r)
23-259	21413235+5732245	—	—	—	w	—	9.2	-11.0 $\pm$ 0.5	7.2	P(r)*

Note. — Spectroscopic Information. For comparison, together with the parameters derived from the high-resolution Echelle spectra included in this work, we include the spectral types and Li EW from low-resolution spectra (Paper I, II). The mark “:” denotes uncertain values. H $\alpha$  EW in parentheses refer to the values obtained from low-resolution spectra. We define the H $\alpha$  type as “c” (standing for CTTS) if broad emission with extended velocity wings was detected, otherwise we name it “w” (standing for WTTS). Whenever the classification based on the H $\alpha$  EW from low-resolution spectra using the criteria in White & Basri 2003 differed from the classification according to line broadening, we include the EW-based result in parentheses (see Sicilia-Aguilar et al. Paper A for more detailed information). The error in the rotational velocity is proportional to the rotational velocity times 1/(1+R), where R indicates the goodness of the cross-correlation. Membership is stated as follows: “Y” = sure member; “P” = probable member, “PN” = probable non-member, “N” = non-member. The label in parentheses indicates whether the membership was obtained from the presence of H $\alpha$  strong emission and/or Li absorption lines (“e”) or via the radial velocity (“r”). A star symbol was added to mark the new members. The label “conf” denotes previous possible members (from low-resolution spectroscopy) that are confirmed as members based on the radial velocities; “rej” denotes previous possible members that are most likely non-members according to radial

velocities. Finally, a comment on binarity (SB2 or SB1) is added in this field.



Table 2. Summary of Disk and Stellar Properties of Members and Probable Members

ID	Sp.Type	Age (Myr)	Mass ( $M_{\odot}$ )	$V \sin i$ (km/s)	$\dot{M}$ ( $10^{-8} M_{\odot}/\text{yr}$ )	Class and Comments
74-48	—	2.4	0.9	$7.6 \pm 1.5$	0	III
73-758	K6.5	1.8	0.8	$7.7 \pm 2.1$	0	Transition
72-1427	M1	2.2	0.5	—	<0.1	II,Ra
81-541	K5.5	2.8	1	—	<0.1	II,Ra
64-156	—	15.6	1.3	$7.4 \pm 1.6$	0	III
73-472	K5	3.3	1.1	$9.6 \pm 2.2$	<0.1	III
73-1059	—	14.4	1	$8.6 \pm 1.4$	0	III
73-311	M1.5	2.8	0.4	—	<0.1	II,B:
73-71	K6	1.8	0.9	$24.4 \pm 5.2$	2.1	II,Ra,Ba
72-875	M0.5	8.4	0.5	$7.0 \pm 2.7$	0	II:,SB1:
61-608	—	10.6	1.2	$8.2 \pm 1.5$	0	III
73-194	K6.5	14.3	0.8	$7.3 \pm 1.7$	0	III
61-893	—	9.4	0.9	$9.9 \pm 3.0$ :	0	III
21360745+5734296	—	—	—	$10.2 \pm 4.2$	0	III:
73-537	G1.5	27.4	1.3	$11.7 \pm 2.9$	0	III
84-23	—	4	1	$9.6 \pm 2$	0	III
21362368+5732452	—	—	—	$7.7 \pm 3.0$ :	0	III:
21362507+5727502	M0	—	—	$7.6 \pm 2.2$	...	II,SB1,B
14-306	K6.5	12.8	0.9	—	0	III
21364596+5729339	—	—	—	$5.7 \pm 2.4$ :	...	I
21364762+5729540	K6	—	—	—	0	III:
14-141	K6	0.6	0.8	$27.0 \pm 8.3$ :	<0.1	II,Ba
14-1229	K6	10.7	0.9	—	0	III
11-2146	K6	0.9	0.9	$12.6 \pm 1.5$	16.2-13.2	II,Za
11-1209	K6	1	0.8	$12.2 \pm 1.1$	0	II,B
21365947+5731349	M0	—	—	—	...	II,Ba
11-1659	K5	5	1.1	$9.1 \pm 1$	0.1273	III:
11-1499	M1.5	1.4	0.4	—	0	III
11-2322	M1	0.8	0.5	$9.5 \pm 2.6$ :	0.80	II,Ba
11-1871	M2	2.5	0.4	—	0.12:	III:
14-222	K7	0.7	0.7	—	0.61-0.86	Transition:
14-287	M0	1	0.6	$11.0 \pm 2.8$	<0.1	II
11-2037	K4.5	2.5	1.3	$8.6 \pm 0.8$	0.97-2.5	II
11-1067	M0.5	2.9	0.5	—	0	III
14-11	M1.5	0.7	0.5	$15.1 \pm 5$	0	Transition
14-125	K5	2.9	1.1	$5.6 \pm 1.5$	<0.1	II,B
11-1513	K7.5	1.2	0.6	—	0	III
11-2131	K6.5	2.3	0.8	—	1.1	II,IPC
11-2487	K7	2.8	0.8	—	0	III
11-2031	K2	2.5	1.7	$12.6 \pm 1.6$	1.6	II
14-103	K7	14.4	0.8	—	0	III
14-197	K5.5	4.2	1	$20.4 \pm 6.5$ :	0	III,SB1:
21372410+5724115	—	—	—	—	...	II,S
14-160	K5	3.1	1.1	$22.5 \pm 4.2$	<0.1	II
14-1017	M0	2.2	0.5	—	<0.1	II,Ra
14-335	K6.5	2.8	0.8	—	...	II

Table 2—Continued

ID	Sp.Type	Age (Myr)	Mass ( $M_{\odot}$ )	$V_{\text{ini}}$ (km/s)	$\dot{M}$ ( $10^{-8}M_{\odot}/\text{yr}$ )	Class and Comments
11-1864	G-K	7.4	1	$9.5 \pm 2.3$	0	III:,SB1
83-343	M0.5	0.9	0.5	$8.8 \pm 2$	...	II :
14-183	K7.0(K5)R	0.9	0.8	$12.8 \pm 4$	$<0.1$	II,SB1:,Ba
14-2148	M1.5	2	0.4	$4.8 \pm 1.7$ :	0	Transition:
21374275+5733250	F9	—	—	—	...	II,Ba
11-1384	K6.5	2.4	0.8	—	0	III
11-383	K5	4.4	0.9	—	$<0.1$	II,S
21374893+5723209	—	—	—	—	...	II,Ba
13-924	K5	4.7	1.1	$8.8 \pm 2$	0	III
12-1984	K6	5.8	0.9	—	0	III
12-2519	K5.5	6.2	1	$10.5 \pm 2.9$	$<0.1$	II
12-1968	K6	2.6	0.9	$10.9 \pm 1.4$	$<0.1$	II+III:, SB2:
12-1422	M0	2.7	0.5	—	0	III
12-1091	G2.5	23.4	1.4	$8.8 \pm 1.2$	0.81-3.3	II,Ba
13-269	K6.5	1.6	0.8	—	0	III
12-583	M0	0.9	0.5	—	0	III
13-1143	—	9.6	1.1	$7.2 \pm 1.1$	0	III
13-1238	M1	0.8	0.5	—	10.7	II,Ba
12-2373	M1	1.8	0.5	$10.0 \pm 2.8$	0	III
82-272	G9	10.5	1.5	$18.1 \pm 5$	23.9	II+II,SB2,S
12-1081	M0.5	4	0.5	—	0	III
13-1161	M0	2.8	0.6	$12.8 \pm 4.0$ :	0	III
12-1613	M1	2.3	0.4	—	0	III
13-1426	M0	1.8	0.5	—	$<0.1$	II,Ba,Za
21380924+5720198	—	—	—	$8.2 \pm 3.2$	...	II,S
13-669	K1	2.8	1.8	$14.2 \pm 1.4$ :	0.59-2.2	II,S
21380979+5729428	—	21380979	0	$9.0 \pm 2.3$		II
13-350	M1	4.2	0.5	$6.4 \pm 1.7$	0	Transition:
12-1017	K5.5	4	1	$8.8 \pm 0.8$	0.06	III
54-1781	M1	2.3	0.4	$7.1 \pm 2.3$	$<0.1$	II
13-1877	K7	1	0.8	—	1.9-2.7	II,Ba
13-277	G1	2.6	2.6	$51.6 \pm 9.4$	30:	II,SB1:,Ba
13-2236	K6.5	5.2	0.9	$15.2 \pm 2.4$	0	III
12-1009	K5.5	2.9	1	$12.6 \pm 2.7$	0	III
94-1119	—	2.6	0.9	$7.3 \pm 0.6$	0	III
13-819	K5.5	2.4	1	—	0.04-0.20	Transition
94-1050	—	16.2	0.9	$7.8 \pm 2.6$	0	III
12-1955	K6.5	6.9	0.9	$9.0 \pm 1.1$	0	III
13-236	K2	2.8	1.7	$9.0 \pm 0.9$	1.5-3.9	II,S
12-2113	K6	1.1	0.9	$11.7 \pm 2.5$	6	II,SB1,S
13-157	K5.5	2.4	1	$8.7 \pm 1.8$	1.6	II,Ba
13-232	M0	2.2	0.6	—	0	III:
21383216+5726359	M0	—	—	—	...	II
13-52	K7	4.1	0.8	$8.1 \pm 1.9$	0	Transition
12-1825	—	4.8	0.5	$8.8 \pm 2.6$	0	III
91-155	M2.5	1.7	0.4	$5.9 \pm 2.4$	...	II

Table 2—Continued

ID	Sp.Type	Age (Myr)	Mass ( $M_{\odot}$ )	$V_{\text{ini}}$ (km/s)	$\dot{M}$ ( $10^{-8} M_{\odot}/\text{yr}$ )	Class and Comments
13-566	K5.5	2.5	0.8	—	0	Transition:
13-1891	M0	5.1	0.5	$10.1 \pm 2.3$	...	II,Za
13-1709	K5.5	5.2	1	$10.4 \pm 2.4$	0.03	III
54-1613	K5	5.2	1.1	$9.5 \pm 0.7$	0.37	Transition:
21384350+5727270	M2	—	—	—	...	Transition
54-1547	K5.5	5.7	1	$20.0 \pm 7.1$	0.21	II,Ra
12-2363	M0.5	0.9	0.5	$27.1 \pm 7.3$	0	III,SB1:
12-595	K7	18.9	0.7	—	0	Transition:
12-1423	K7	2.3	0.8	$7.5 \pm 1.5$	$< 0.1$	III
12-1010	M2	5.3	0.4	$8.2 \pm 2.3$	...	II,S
12-2098	M2.5	2.2	0.4	—	0	III
21-851	—	25.6	0.9	$6.0 \pm 2.4$	0	III
13-1087	K4	4.2	1.4	$11.2 \pm 0.8$	0.28-0.37:	III:
91-506	K6.5	2.5	0.8	$8.4 \pm 2.1$	0.14	II,Ra
24-692	M1	2.7	0.5	$6.0 \pm 1.9$	0	III,SB1
12-1027	M0	2.6	0.4	—	0	III
24-77	K6.5	7.4	0.9	—	0	III
24-108	K5.5	4.3	1	—	0	III
12-1617	M1	1.2	0.5	$6.1 \pm 2.3$ :	0.88	II
13-1048	M0	7.4	0.6	$10.9 \pm 1.4$	$< 0.1$	II,Za
13-1250	K4.5	3.3	1.3	$8.3 \pm 0.8$	0.10	Transition,IPC
21-563	M1	1.4	0.6	—	...	III
12-942	K7.5	1.5	0.7	$19.3 \pm 3.8$	0	III
91-815	M2	2	0.4	$6.5 \pm 2.2$	0	III
21-1590	K7	3.4	0.8	$10.6 \pm 2$	0	III
21392541+5733202	—	—	—	$8.8 \pm 1$	...	Transition,S
21392570+5729455	—	—	—	$7.5 \pm 2.3$	...	Transition
24-542	K4	2.3	1.1	—	0	III
21393104+5747140	—	—	—	$8.8 \pm 0.5$	...	II,S
24-515	M0.5	2.8	0.5	$7.6 \pm 2.6$ :	$< 0.1$	Transition
21-998	K5.5	5.6	1	$7.3 \pm 2.8$	0.73	II,SB1:
21-33	M0	4	0.5	$8.9 \pm 3.1$ :	$< 0.1$	II,S
24-170	K7.5	2.4	0.7	$7.0 \pm 2.9$ :	0	III:
53-1803	K6.5	20.5	0.8	$7.2 \pm 1.6$	0	III,SB1
24-48	M0.5	2.4	0.5	$8.1 \pm 1.1$	0	III
92-1198	—	2.3	1	$14.1 \pm 1.6$	0	III
21-230	M0.5	2.5	0.5	$11.3 \pm 2.1$	0	III
92-393	M2	0.9	0.4	$14.2 \pm 4.1$	$< 0.1$	Transition,Za
24-820	K6.5	26.7	0.8	$6.9 \pm 1.4$	0	III
21-2251	M2	1.3	0.4	$16.7 \pm 5.9$ :	0	III,SB1:
21-1586	K7	3.9	0.6	$9.4 \pm 2.5$	0	III
24-78	M2	1.4	0.4	$12.0 \pm 3.8$ :	0	III
92-1162	M2	1.6	0.4	$8.0 \pm 2.1$ :	0	III
53-1762	M0	3	0.6	$8.0 \pm 2.8$ :	0.434	II:,SB1:
24-1047	—	2.3	1	$14.7 \pm 1.7$ :	0	III
93-361	G1	15.6	1.5	—	$< 0.1$	II,Za

Table 2—Continued

ID	Sp.Type	Age (Myr)	Mass ( $M_{\odot}$ )	$Vsini$ (km/s)	$\dot{M}$ ( $10^{-8}M_{\odot}/\text{yr}$ )	Class and Comments
21395813+5728335	—	—	—	$11.8 \pm 1$	...	II,S
21-1692	M1	2.5	0.5	$8.9 \pm 1.6$	0	III
21-763	M0	2.6	0.6	$28.3 \pm 8.1$	0	III
24-817	K6.5	4.6	0.9	$15.0 \pm 2.9$	0	III
21-895	K5	2.8	1.1	—	0:	III:
21-1762	K5	4.3	1.1	$12.3 \pm 1.7$	0.23	III
93-720	—	1.8	1	$12.5 \pm 1.1$	...	II,Ra
24-382	K7.5	6	0.7	$8.4 \pm 1.2$	0	III
24-1736	M1	3.9	0.4	$6.9 \pm 2.4$ :	0.18	II,Ra
24-1796	K7	6	0.8	$13.2 \pm 5.6$ :	0.31-0.55	II+II, SB2:
21401438+5740507	—	—	—	$8.7 \pm 2.4$	...	II,Ba
22-2651	M1.5	3.9	0.4	—	<0.1	II,Za
21402192+5730054	K6	—	—	$10.6 \pm 1$	...	Transition,IPC
92-1103	K5.5	1.2	1	$9.0 \pm 2.2$	<0.1	II:
22-1418	M1.5	2.1	0.4	$10.7 \pm 2.1$	<0.1	II:
23-405	K5	5	1.1	$12.8 \pm 1.6$	<0.1	II,Za
23-570	K6	4.2	0.9	$8.2 \pm 0.8$	0.62	II,Ba
93-540	M0	2.3	0.6	$7.6 \pm 1.9$	<0.1	II
53-1843	M0.5	3.6	0.5	$11.4 \pm 2.8$	0	III
93-168	K6.5	2.5	0.8	$8.3 \pm 1.1$	0.05	II,Za
92-926	—	6.9	1.3	$6.9 \pm 0.5$	0	III
23-162	K7	6.6	0.8	$7.4 \pm 1.1$	<0.1	II
23-753	M0.5-M0	8.5	0.5	$8.3 \pm 2.2$	0	III
53-1561	K6	3	0.8	$8.1 \pm 1.9$	...	II,Za
22-445	M0.5	2.4	0.5	$19.9 \pm 5.9$	0	III
22-1526	M1	3.2	0.5	$9.9 \pm 2.3$	0	III
23-1282	—	6.7	1.1	$8.8 \pm 1.1$	0	III
23-969	K5.5	2.9	1	$10.9 \pm 1.1$	0.41	II,Za
22-960	M2.5	2.5	0.4	—	0	III
22-1569	M1	1.3	0.5	$7.5 \pm 1$	...	III:
23-798	K6	14.7	0.9	$6.1 \pm 2.2$ :	0.79	II,Ba
23-259	—	2.2	1.1	$7.2 \pm 0.7$	0	III

Note. — Summary of the properties of the stars in Tr 37. Only the star being sure or probable members are displayed here. Ages and masses are derived from the V vs. V-I diagram, using the isochrones by Siess et al. 2000 (see Paper I, Paper II for a detailed description of spectral typing and age/mass calculation). Errors in the  $Vsini$  are derived as  $Vsini/(1+R)$  (see Tonry & Davis 1979; Hartmann et al. 1986). The best estimate of the accretion rate is selected for this summary. Whenever accretion rates derived from U band photometry were available (Paper II), we included them. Since some stars had been observed in U band in two campaigns, we include both values. As in the text, we denote with  $\dot{M}=0$  those stars with no U excess and  $H\alpha$  profiles consistent with diskless WTTS or Class III objects. For stars with no detectable U excess but broad profiles, we give an upper limit to accretion of  $<0.1 \cdot 10^{-8} M_{\odot}/\text{yr}$  (see text). We do not provide an accretion value for stars not observed in U band and broad or probably broad  $H\alpha$  profiles. For the exceptional star 13-277, whose spectral type is uncertain due to veiling, we provide an approximate accretion rate from the  $H\alpha$  width at 10% maximum (see text). Most of these stars without a value for accretion are likely to be accreting (showing broad profiles, see figures). The comments include the class (I, II, III or Transition object), the binarity (SB1= single-lined spectroscopic binary; SB2= double-lined spectroscopic binary), and the details on the  $H\alpha$  profile (Ba= blue-shifted absorption; Ra= red-shifted absorption; Za= absorption with approximately zero velocity shift; B= blue-shifted emission; R=red-shifted emission; IPC= inverse P-Cygni

profile). Uncertain values are denoted by “:”.